The Veliger 42(3):218–248 (July 1, 1999)

THE VELIGER

Bathymodiolus (Bivalvia: Mytilidae) from Hydrothermal Vents on the Azores Triple Junction and the Logatchev Hydrothermal Field, Mid-Atlantic Ridge

RUDO VON COSEL

Muséum National d'Histoire Naturelle, Paris, 55, rue de Buffon, F-75005 Paris, France

THIERRY COMTET

Centre IFREMER de Brest, Département Environnement Profond. B.P. 70, F-29280 Plouzané, France

AND

ELENA M. KRYLOVA

Institute of Oceanology, Russian Academy of Sciences, Moscow

Abstract. *Bathymodiolus* ***azoricus*** n. sp. is described from the Lucky Strike (31°17′N) and the Menez Gwen (37°50′N) hydrothermal fields on the Azores Triple Junction, Mid-Atlantic Ridge, and another species, *Bathymodiolus* sp. aff. *B. puteoserpentis* from Logatchev (14°45′N) hydrothermal field is treated but not named. Both species are compared with *B. puteoserpentis* Cosel, Métivier & Hashimoto, 1994, from the Snake Pit area (23°22′N), also on the Mid Atlantic Ridge. *B.* ***azoricus*** is very variable but well distinguished from *Bathymodiolus* sp. and *B. puteoserpentis* by its almost terminal umbo. The three species differ from the type species *B. thermophilus* principally by the absence of an inner mantle fusion and a very short valvular siphonal membrane. The slight differences between *B. puteoserpentis* and *Bathymodiolus* sp. from the Logatchev field do not warrant separation of the latter on species level. The specific endemism of Mytilidae along the Mid-Atlantic Ridge is discussed.

INTRODUCTION

Bathymodiolus species are mytilid bivalves which live in both hydrothermal vent and cold-seep environments using chemoautotrophic processes for their metabolism (Childress & Fisher, 1992). Since the discovery of *Bathymodiolus thermophilus* Kenk & Wilson, 1985, on the Galapagos Rift in 1977, 11 other species of the genus *Bathymodiolus* have been described from a variety of hydrothermal vent and cold-seep environments of both the Pacific and Atlantic oceans (Cosel et al., 1994; Hashimoto & Okutani, 1994; Cosel & Olu, 1998; Gustafson et al., 1998).

On the Mid-Atlantic Ridge, the vent mytilid *Bathymodiolus puteoserpentis* Cosel, Métivier & Hashimoto, 1994, was first collected on the Snake Pit hydrothermal field (23°22′N), in June 1988, during the French HYDROSNAKE expedition (Cosel et al., 1994). Subsequently, *Bathymodiolus*-like mussels were found also on other localities of this ridge.

The next site on the Mid-Atlantic Ridge (further abbreviated as MAR) with a mussel population was discovered in September 1992 at 37°17.6′N by an American expedition, and samples were taken by dredge (Van Dover, 1995). In 1993, more mytilids were collected at the same locality, then called Lucky Strike hydrothermal field (37°17′N, 1640–1700 m) by the submersible Alvin during

→

Explanation of Figures 1–5

Figures 1–5. *Bathymodiolus* ***azoricus*** Cosel & Comtet, sp. nov. Figure 1. Holotype, MNHN, 111.9 mm. PP11 site, Menez Gwen hydrothermal field Mid-Atlantic Ridge, 37°50.5′N, 31°31.3′W, 866 m, DIVA 2, dive 13. Exterior and interior of both valves, dorsal view of specimen and ventral view of right valve to show the position of foot/byssus retractor scars. Figure 2. Paratype, ZMM, 94.3 mm. Same locality. Exterior of left valve. Figure 3. Paratype, MNHN, 109.7 mm. Same locality. Exterior and interior of left valve. Figure 4. Paratype, MNHN, 103.0 mm. Same locality. Exterior and interior of right valve. Figure 5. Specimen from Menez Gwen, same locality, DIVA 2, dive 11, MNHN, 70.4 mm. Exterior and interior of left valve.


1
2
3
4
5

the American expedition LUCKY STRIKE 1993 (Van Dover et al., 1996). Additional populations of this mussel were found and specimens collected on a larger scale by the French submersible Nautile during the expeditions DIVA 1 (May 1994) and DIVA 2 (June 1994) of the R/V *Nadir*. During these cruises, also the newly discovered Menez Gwen hydrothermal field (37°50′N, 844–850 m) was studied and mussels were collected (Desbruyères et al., 1994; Fouquet et al., 1995).

Another mussel population was discovered in June 1993 at 29°10′N (3080 m) on the Broken Spur vent field during the ATLANTIS II cruise (Murton et al., 1995). The two examined shells, brought to our attention by Eve Southward, were provisionally identified as *Bathymodiolus puteoserpentis* by the first author.

Vent mussels were also found in July 1994 at 14°45′N by the Russian LOGATCHEV-7 expedition on board the R/V *Professor Logatchev* (Batuyev et al., 1994). A few mussels were sampled by TV-guided bottom grab. More material, in total 15 specimens, was taken in February 1995 by the Russian submersible Mir-2 during the cruise 35 of the R/V *Akademik Mstislav Keldysch* at 14°50′N. In December 1995, specimens of the same mussel were taken by the French submersible Nautile during the cruise MICROSMOKE at 14°45′N, now called the Logatchev hydrothermal vent field.

The two *Bathymodiolus* species from 37°N (Lucky Strike and Menez Gwen hydrothermal field, Azores Triple Junction) and from the Logatchev hydrothermal field were found to be different from *Bathymodiolus puteoserpentis* and are described in this paper, but only one of them is introduced as a new species. Some ecological and biogeographical remarks on mytilids of the MAR are also given.

MATERIALS AND METHODS

Most of the studied material was collected during the already mentioned French expeditions DIVA 1 and DIVA 2, organized by IFREMER (Institut français de Recherche pour l'Exploitation de la Mer) and MICROSMOKE, organized by the CNRS (Centre National de Recherches Scientifiques). The material was sorted by the Centre National de Tri d'Océanographique Biologique (CENTOB), Brest.

Shell lengths and heights were measured using the standards of Kenk & Wilson (1985:fig. 1) in a total of 7832 individuals from both Azores Triple Junction and Logatchev. Anterior part length (i.e., length from the anterior margin to the umbo) was additionally measured on 159 individuals. Data for *Bathymodiolus puteoserpentis* were taken from Cosel et al. (1994) and from measurements of a few additional specimens. All statistical analyses were carried out using StatView II™ or Microsoft Excel 5.0.

Abbreviations used in the text: LACM—Los Angeles County Museum of Natural History, Los Angeles; MCZ—Museum of Comparative Zoology at Harvard University, Cambridge, Massachusetts; MNHN—Muséum National d'Histoire Naturelle, Paris, France; NMNZ—National Museum of New Zealand, Wellington, New Zealand; NSMT—Natural Science Museum, Tokyo, Japan; SMF—Natur-Museum und Forschungsinstitut Senckenberg, Frankfurt/M, Germany; USNM—National Museum of Natural History, Smithsonian Institution, Washington, D.C.; ZMM—Zoological Museum of Moscow University. sh.—empty shell; spm.—wet preserved specimen(s); R/V—research vessel; MAR—Mid-Atlantic Ridge.

SYSTEMATICS

Family MYTILIDAE

Genus *Bathymodiolus* Kenk & Wilson, 1985

Bathymodiolus azoricus Cosel & Comtet, sp. nov. (Figures 1–15, 25–33, 36, 37, 39–52, 59, 60, 62)

Type material: Holotype, MNHN, Menez Gwen hydrothermal field, Mid-Atlantic Ridge, DIVA 2 expedition, dive 13, A.-M. Alayse, observer, 15 June 1995. 22 paratypes with preserved animal, same locality, 14 in MNHN; 1 in MCZ; 1 in NSMT; 1 in USNM; 1 in LACM; 1 in SMF; 1 in ZMM; 1 in Museum Funchal; 1 in NMNZ.

Type locality: PP11 site, 37°50.5′N, 31°31.3′W, 866 m,

→

Explanation of Figures 6–11

Figures 6–11. *Bathymodiolus azoricus* Cosel & Comtet, sp. nov. Figure 6. Specimen from Lucky Strike hydrothermal field, 64.0 mm, site Statue of Liberty, 37°17.59′N, 32°16.50′W, 1635 m, "LUCKY STRIKE 1993" expedition, dive 2605. Exterior and interior of left valve. Figure 7. Specimen from Lucky Strike hydrothermal field, 44.8 mm. Same locality. Exterior and interior of left valve. Figure 8. Specimen from Lucky Strike hydrothermal field, site Pagoda (PP7), 37°17.63′N, 32°16.96′W, 1629 m, DIVA 2, dive 07, 91.1 mm. Exterior, interior, and ventral inner view of left valve. Figure 9. Specimen from Lucky Strike hydrothermal field. Same locality, 59.3 mm. Exterior of right valve. Figure 10. Specimen from Lucky Strike hydrothermal field, site Eiffel Tower, 37°17.32′N, 32°16.52′W, 1685 m, DIVA 2, dive 08, 84.7 mm. Exterior, interior, and ventral inner view of left valve. Figure 11. Specimen from Lucky Strike hydrothermal field, site Elisabeth, 37°17.63′N, 32°16.87′W, 1640 m, DIVA 2, dive 24, 114.1 mm. Exterior and interior of left valve. All specimens MNHN.

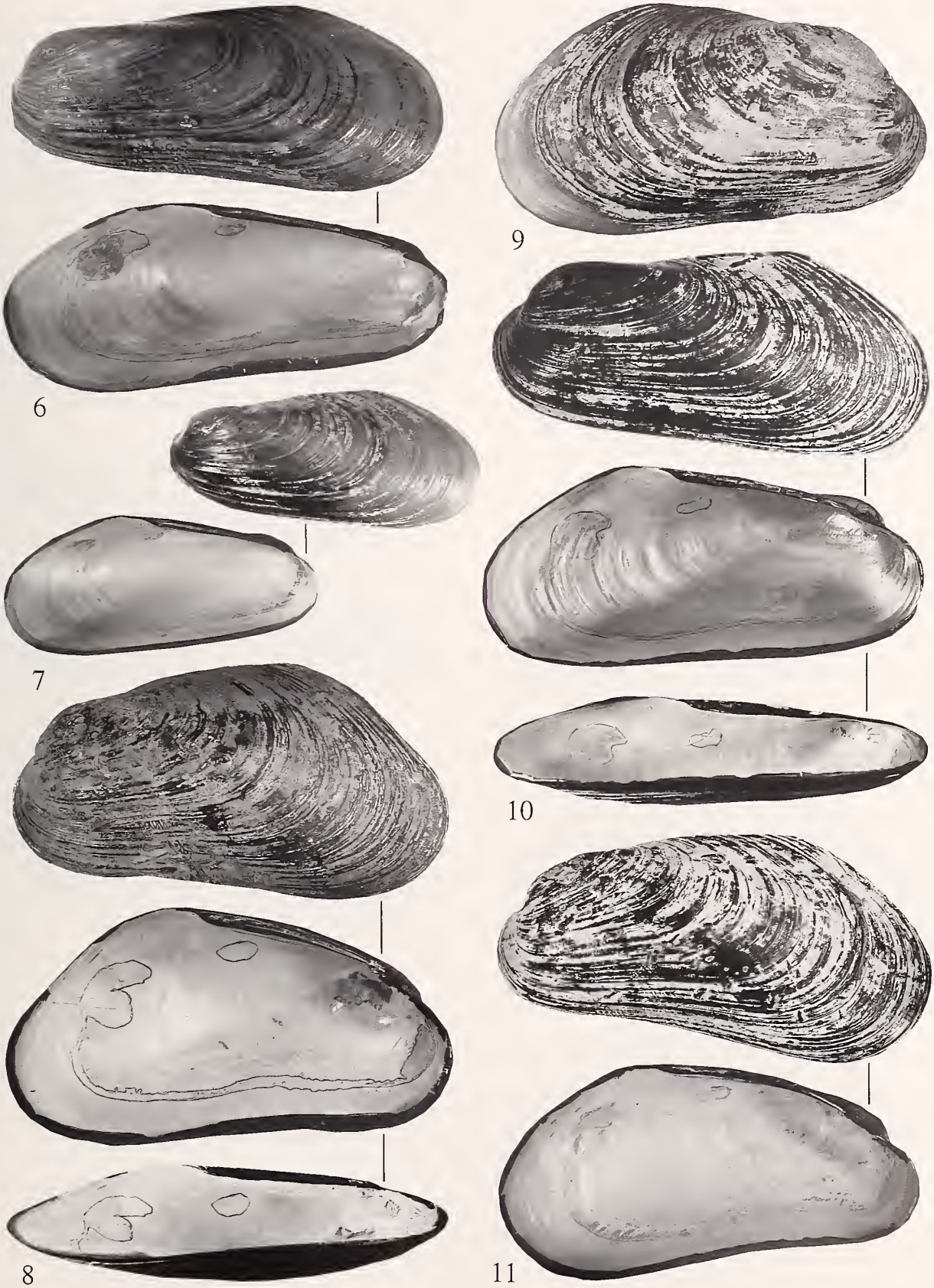
6
7
8
9
10
11

Menez Gwen hydrothermal field, Azores Triple Junction, Mid-Atlantic Ridge.

Description: Shell up to 119 mm long, more or less elongate-modioliform, from thin but solid to rather thick, extremely variable in outline and length/height ratio, but also in tumidity and shell thickness, equivalve, smaller specimens often shorter. Beaks subterminal to almost terminal. Anterior margin more or less broadly rounded; ventral margin in juvenile, half-grown, and subadult specimens mostly more or less convex or straight, in fully grown specimens straight or more or less concave. Postero-ventral margin evenly rounded, postero-dorsal margin slightly to markedly convex, occasionally straight; postero-dorsal corner rounded; ligament plate usually slightly arched but occasionally almost straight. Exterior with more or less dense, irregular growth lines and growth waves, more or less reflected on interior (see Figures 1 and 10). Some specimens have about five to six broad and very obscure transverse waves in middle of shell which cause occasionally undulation of concentric striae and may be marked by darker color of periostracum; they are reflected as very flat and indistinct waves on interior (see Figure 4). In very few specimens, sculpture of faint, broad, radial and sometimes bifurcating undulations visible on postero-dorsal slope slightly visible on Figure 6; it may be very slightly reflected on inside. Umbo broad, somewhat flattened.

Shell without periostracum dull whitish; interior nacreous white.

Periostracum strong, warm chestnut brown, in umbonal region and often also lighter brown postero-dorsally; smaller specimens especially often appear more or less two-colored with antero-ventral part dark chestnut brown and postero-dorsal part lighter olive brown with relative sharp limit reaching from umbonal region to postero-ventral corner or just in front of it. Surface somewhat dull, with no periostracal hairs; however, byssal endplates of other specimens scattered over whole valve.

Hinge edentulous, anterior hinge margin, however, slightly protruding toward ventral. Ligament opisthodetic, strong, extending over whole postero-dorsal margin nearly to postero-dorsal corner and ending abruptly or in a taper. Subligamental shell ridge hardly marked to obsolete from under umbos to middle of ligament, then missing. Anterior adductor scar long-oval, arched, situated just in front of umbo. Posterior adductor scar united with posterior scar of posterior pedal and byssus retractor muscle. Anterior scar of same muscle separated and situated under ligament's end or slighty more forward. Anterior byssus retractor muscle scar situated in umbonal cavity, reaching from umbo toward posterior, visible only in posterior and ventral view but not in lateral view of interior. Pallial line ventrally slightly concave or straight.

Examined larval shells (Figures 45–52) measured between 522 and 527 μm long and were nearly 500 μm high. There is a separation between a very small protoconch I (about 110 μm long) and the large protoconch II, which indicates a long planktonic larval phase. Protoconch II pale beige-salmon and well separated from teleoconch which in ultra-juvenile specimens is nearly transparent. Surface of protoconch II with fine regular concentric grooves which are more or less densely spaced, protoconch I with irregular sculpture.

Animal with very large ctenidia which are nearly four-fifths of shell length; outer and inner demibranch almost of equal size, outer demibranch only slightly shorter anteriorly. Ascending lamellae of both demibranchs anteriorly fused to the mantle visceral mass for a very short distance, then becoming free toward posterior. Narrow and well-visible food groove on ventral edge of each demibranch; outer surface of ascending lamellae of inner and outer demibranch with grooves just below free edges and parallel to them. No muscular longitudinal ridge on mantle and visceral mass where dorsal edges of ascending lamellae touch mantle lobes. Connection bars between free edges and gill axes absent. Inner mantle folds separate along whole ventral margin length from anterior adductor to posterior margin. Filaments moderately broad; each fifth to seventh filament with a connecting septum of about half the height of demibranchs.

Mantle lobes thin but with strongly muscular mantle margins. Mantle edges with three folds, inner mantle fold frilled but degree of frilling variable. On anterior end, inner mantle folds pass from ventrally over anterior adductor muscle up- and foreward along anterior margin, then fold down- and backward to pass again lower end of anterior adductor muscle or slightly posterior to it toward ventral margin. On this "folding part" mantle edge

→

Explanation of Figures 12–15

Figures 12–15 *Bathymodiolus* ***azoricus*** Cosel & Comtet, sp. nov. Figure 12. Specimen from Lucky Strike hydrothermal field, site PP5, 37°17.49′N, 32°16.88′W, 1725 m, DIVA 2, dive 05, 83.0 mm. Exterior, interior, and ventral inner view of right valve and dorsal view of specimen. Figure 13. Specimen from Lucky Strike hydrothermal field. Same locality, 63.1 mm. Exterior, interior, and inner ventral view of left valve. Figure 14. Specimen from Lucky Strike hydrothermal field. Same locality, 61.6 mm. Exterior and interior of left valve, dorsal view of specimen. Note the different tumidity of the specimens on Figures 13 and 14 from the same locality. Figure 15. Specimen from Lucky Strike hydrothermal field. Same locality, 90.3 mm. Exterior and interior of left valve. All specimens MNHN.

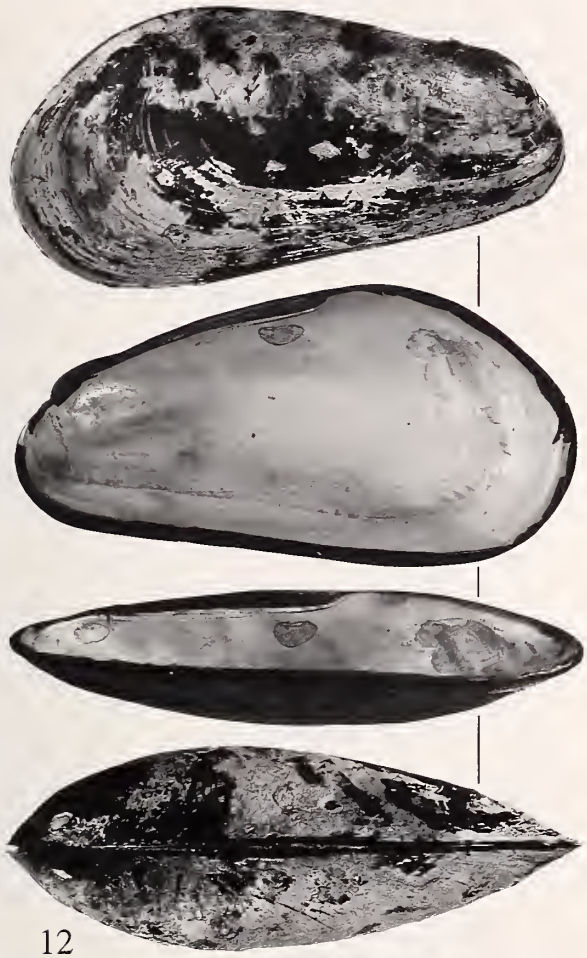

12

14

13

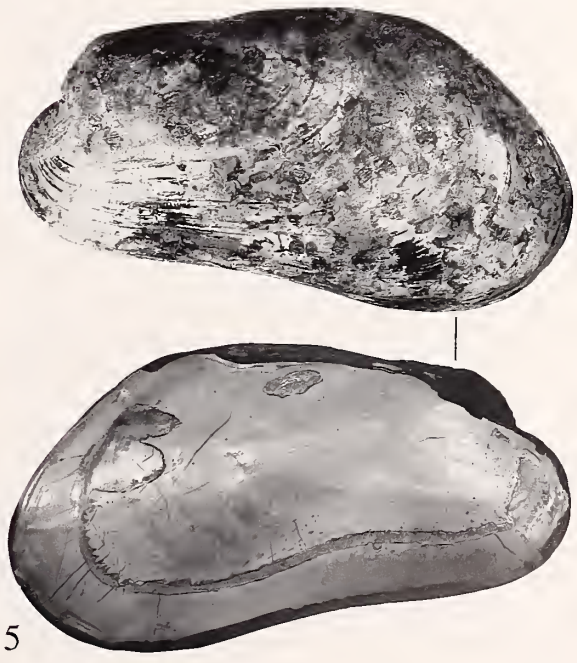

15

remains frilled (Figure 33), but occasionally is less or not frilled on passage over anterior adductor from one valve to the other (Figures 31, 32). Valvular siphonal membrane short and rather strong, reaching from postero-ventral corner to exhalent siphonal opening, with more or less developed papilla in middle on anterior edge (see Figures 31–33). Inner siphonal aperture with internal diaphragm with horizontal slit and muscular fold around it. Two very broad and short flattened tentacles ventrally under slit, directed toward anus (see Figures 43, 44).

Foot somewhat variable but generally rather small and quite slender, with ventral byssal groove two-thirds to three-fourths length of foot. Foot-byssus retractor muscle complex with rather long anterior retractor; posterior byssus retractors consisting of two quite strong, diverging muscle bundles with common base at base of byssus. Anterior bundle very short and broad and arising rather steeply toward attachment point on shell inside, posterior bundle very long and thin, passing almost parallel to longitudinal shell axis toward attachment point directly in front of posterior adductor. Posterior foot retractor rather thin, arising from base of foot, well in front of base of byssus retractor muscles, passing outer side of anterior retractor toward anterior bundle of posterior byssus retractor; it reaches inner shell surface closely appressed to anterior bundle over half to two-thirds its length. Labial palps variable in size, generally rather large (Figure 42) but in juveniles more or less small, occasionally also in larger specimens (Figure 41). Posterior labial palps narrow-triangular, anterior two slightly smaller than posterior pair and still narrower. Labial palp suspensor muscles present.

Mouth transverse, slit-shaped; esophagus a narrow tube with irregular, close-set longitudinal ridges on its inner surface just in front of entrance to stomach. Stomach (Figure 62) small and very elongate for a mytilid, with thin walls, anterior chamber slightly shorter than posterior chamber but both with about equal width. Digestive diverticula around whole stomach. Style sac and midgut conjoined. Major typhlosole passing from there toward anterior along floor of posterior stomach chamber, and ending in anterior chamber. On left side of posterior chamber, three diverticle ducts open into shallow depression corresponding to left pouch and situated below gastric shield. Small grooves leading from every digestive duct opening and joining to form beginning of intestinal groove. This latter following major typhlosole, turning right and running along right side of it toward and into midgut. Minor typhlosole on right side of midgut and ending just after entering posterior chamber. In this chamber six openings of digestive diverticula ducts. Stomach of examined specimen contained only some mucus. No crystal style found.

Midgut running straight backward to under ventricle, there making very small to moderately large counterclockwise recurrent loop before entering it just in front of auricular ostiae. Heart with muscular ventricle and very large auricles which are fused posteriorly under intestine.

Selected measurements (length, height, tumidity) in mm with length-height ratios:

a) Menez Gwen

111.9 × 47.4 × 36.0	Menez Gwen Pl 13	2.4	holotype MNHN
109.7 × 45.8 × 34.7	Menez Gwen Pl 13	2.4	paratype MNHN
109.0 × 49.4 × 41.3	Menez Gwen Pl 13	2.2	paratype USNM
108.7 × 49.6 × 38.2	Menez Gwen Pl 13	2.2	paratype MNHN
108.0 × 45.8 × 39.1	Menez Gwen Pl 13	2.4	paratype MNHN
107.5 × 49.5 × 39.6	Menez Gwen Pl 13	2.2	paratype MNHN
103.0 × 44.1 × 35.7	Menez Gwen Pl 13	2.3	paratype MNHN
100.3 × 42.3 × 37.8	Menez Gwen Pl 13	2.4	paratype MNHN
98.5 × 44.2 × 33.2	Menez Gwen Pl 13	2.2	paratype MNHN
95.8 × 38.0 × 29.4	Menez Gwen Pl 13	2.5	paratype SMF
95.2 × 44.7 × 35.1	Menez Gwen Pl 13	2.1	paratype MCZ
95.0 × 40.0 × 34.9	Menez Gwen Pl 13	2.4	paratype MNHN
94.3 × 44.1 × 35.5	Menez Gwen Pl 13	2.1	paratype ZMM
93.4 × 42.6 × 31.7	Menez Gwen Pl 13	2.2	paratype Funchal Mus.
93.0 × 44.1 × 36.9	Menez Gwen Pl 13	2.1	paratype MNHN
92.7 × 40.3 × 33.2	Menez Gwen Pl 13	2.3	paratype LACM
90.9 × 38.7 × 34.5	Menez Gwen Pl 13	2.3	paratype MNHN
87.6 × 40.4 × 30.0	Menez Gwen Pl 13	2.2	paratype MNHN
83.8 × 36.0 × 28.0	Menez Gwen Pl 13	2.3	paratype MNHN
79.6 × 35.0 × 27.8	Menez Gwen Pl 13	2.3	paratype NSMT
77.7 × 32.1 × 27.6	Menez Gwen Pl 13	2.4	paratype MNHN
76.0 × 32.7 × 25.4	Menez Gwen Pl 13	2.3	paratype NMNZ
62.9 × 30.3 × 25.7	Menez Gwen Pl 13	2.1	paratype MNHN

b) Lucky Strike

119.3 × 52.7 × 46.4 mm	Elisabeth Pl. 24	2.3
113.8 × 56.2 × 45.1 mm	Elisabeth Pl. 24	2.0
101.4 × 45.7 × 38.7 mm	Eiffel Tower Pl 08	2.2
97.0 × 43.5 × 33.4 mm	Eiffel Tower Pl 08	2.2
96.0 × 44.0 × 42.0 mm	pp7 Pagoda	2.2
94.6 × 45.1 × 40.0 mm	Eiffel Tower Pl 08	2.1
94.5 × 42.6 × 37.4 mm	pp7 Pagoda	2.2
91.1 × 47.4 × 37.0 mm	pp7 Pagoda	1.9
90.7 × 40.0 × 34.7 mm	Eiffel Tower Pl 08	2.3
89.4 × 43.3 × 32.0 mm	Eiffel Tower Pl 08	2.1
88.4 × 40.4 × 33.3 mm	pp7 Pagoda	2.2
85.4 × 37.0 × 37.0 mm	pp7 Pagoda	2.3
84.1 × 42.7 × 33.6 mm	Eiffel Tower Pl 08	2.0
82.0 × 38.6 × 32.9 mm	pp7 Pagoda	2.1

81.1 × 37.5 × 31.1 mm	pp7 Pagoda	2.2
76.0 × 37.2 × 31.3 mm	pp7 Pagoda	2.0
71.7 × 40.6 × 31.0 mm	pp7 Pagoda	1.8
67.3 × 29.8 × 28.6 mm	pp7 Pagoda	2.3
61.1 × 28.4 × 24.7 mm	pp7 Pagoda	2.2
52.4 × 28.4 × 25.2 mm	pp7 Pagoda	1.8
57.8 × 30.3 × 27.7 mm	pp7 Pagoda	1.9
47.8 × 25.5 × 24.5 mm	pp7 Pagoda	1.9
44.9 × 23.1 × 17.5 mm	Pl 10 Eiffel Tower	1.9

Material examined: Type material; other material: Mid-Atlantic Ridge, Azores Triple Junction, Menez Gwen hydrothermal field, site PP11, 37°50.5′N, 31°31.3′W, 866 m, DIVA 2, dive 11, M. Biscoito, observer, 14 June 1995, 46 spm.; site Mogued-Gwen (PP10) 37°50.56′N, 31°31.27′W, 877 m, DIVA 1, dive 13, sample 13.6, Y. Fouquet, observer, 21 May 1994, 3 spm.; same locality, DIVA 2 dive 12, D. Desbruyères, observer, 14 June 1995, 15 spm.; Lucky Strike hydrothermal field, site Statue of Liberty, 37°17.59′N, 32°16.50′W, 1635 m, expedition "LUCKY STRIKE 1993," dive 2605, D. Desbruyères and D. Colodner, observers, 31 May 1993, 29 spm.; site Sintra, 37°17.57′N, 32°16.57′W, 1622 m, DIVA 2, dive 02, Ph. Crassous, observer, 4 June 1995, 26 spm., 10 juv. spm.; site Eiffel Tower, 37°17.32′N, 32°16.52′W, 1685 m, DIVA 2, dive 08, Th. Comtet, observer, 10 June 1995, 19 spm.; same locality, dive 10, M.-C. Fabri, observer, 12 June 1995, 25 spm, 10 juv. spm.; site Isabel, 37°17.37′N, 32°16.64′W, 1685 m, DIVA 2, dive 01, A.-M. Alayse, observer, 3 June 1995, 15 spm., 3 juv. spm.; same locality, dive 03, 8 juv. spm.; site Pagoda (PP 7), 37°17.63′N, 32°16.96′W, 1629 m, DIVA 2, dive 06, P. Briand, observer 8 June 1995, 11 spm, 8 juv. spm.; same locality, dive 07, P.-M. Sarradin, observer; 9 June 1995, 37 spm., 2 v. and numerous juveniles; site PP 5, 37°17.49′N, 32°16.88′W, 1725 m, DIVA 2, dive 05, F. Barriga, observer, 7 June 1995, 15 spm, 13 juv. spm.; site Elisabeth 37°17.63′N, 32°16.87′W, 1640 m DIVA 2 dive 24, A.M. Alayse, observer, 30 June 1995, 15 spm., all MNHN.

Biotope: *Bathymodiolus* ***azoricus*** dominates the fauna of both the Menez Gwen and Lucky Strike hydrothermal fields. At Lucky Strike, the mussels live byssally attached to hard substrate and cover the walls of active edifices and flanges (on the Pagoda site), where small specimens reach densities up to 10,000 ind/m^2 (A. Colaço, personal communications). They also colonize cracks in the sea floor. The species lives at temperatures ranging from about 6°C (i.e., the ambient seawater temperature) to about 30°C. The distribution of the mussels along the thermal and chemical gradient seems to be related to their size, the largest individuals living in the warmest areas (Comtet, unpublished data). At Menez Gwen, the colo-

→

Explanation of Figures 16–21

Figures 16–21 *Bathymodiolus* sp. Figure 16. Specimen from Logachev hydrothermal field, 14°45′N, 44°58′W, 2930–3010 m, cruise 35 R/V *Akademik Mstislav Keldysch,* sta. 3452, ZMM, 61.5 mm, exterior and interior of left valve, exterior of right valve. Figure 17. Specimen from Logatchev hydrothermal field. Same locality, 83.3 mm. Interior and exterior of right valve. MNHN. Figure 18. Specimen from Logatchev hydrothermal field, Irina site 14°45.10′N, 44°48.60′W, 3040 m, MIKROSMOKE, dive 21, 69.1 mm. Exterior and interior of left valve. Figure 19. Specimen from Logatchev hydrothermal field. Same locality, 122.9 mm. Exterior of both valves, interior of right valve. Figure 20. Specimen from Logatchev hydrothermal field. Same locality, 47.5 mm. Exterior of left valve. Figure 21. Specimen from Logatchev hydrothermal field. Same locality, 41.1 mm. Exterior of left valve. All MNHN.

Explanation of Figures 22–30

Figures 22–24 *Bathymodiolus* sp. Figure 22. Specimen from Logatchev hydrothermal field, Irina site, 14°45.10′N, 44°48.60′W, 3063 m, MIKROSMOKE, dive 20, 95.0 mm. Exterior, interior, and inner ventral view of right valve, dorsal view of specimen. Figure 23. Specimen from Logatchev hydrothermal field, Irina site 14°45.10′N, 44°48.60′W, 3040 m, MICROSMOKE, dive 21, 120.3 mm. Exterior and interior of left valve. Figure 24. Specimen from Logatchev hydrothermal field. Irina site, 14°45.10′N, 44°48.60′W, 3063 m, MICROSMOKE, dive 20, 81.7 mm. Exterior of left valve. All MNHN. Figures 25–30. *Bathymodiolus* ***azoricus*** Cosel & Comtet, sp. nov. Figure 25. Specimen from Lucky Strike hydrothermal field, site Pagoda (PP7), 37°17.63′N, 32°16.96′W, 1629 m, DIVA 2, dive 07, 44.4 mm. Exterior and interior of left valve. Figure 26. Specimen from Lucky Strike hydrothermal field, same locality, 34.6 mm. Exterior and interior of left valve. Figure 27. Specimen from Lucky Strike hydrothermal field, site PP 5, 37°17.49′N, 32°16.88′W, 1725 m, DIVA 2, dive 05, 47.3 mm. Exterior and interior of left valve. Figure 28. Specimen from Lucky Strike hydrothermal field, site Eiffel Tower, 37°17.32′N, 32°16.52′W, 1685 m, DIVA 2, dive 10, 48.3 mm. Exterior and interior of left valve. Note the highly different height of specimens of the same size. Figure 29. Specimen from Lucky Strike hydrothermal field, site Pagoda (PP7), 37°17.63′N, 32°16.96′W, 1629 m, DIVA 2, dive 07, 16.2 mm. Exterior of left valve. Figure 30. Specimen from Menez Gwen hydrothermal field, site Mogued Gwen (PP10) 37°50.56′N, 31°31.27′W, 877 m, DIVA 2, dive 12, 85.0 mm (details of this specimen shown on Figures 31 and 36). All specimens MNHN.

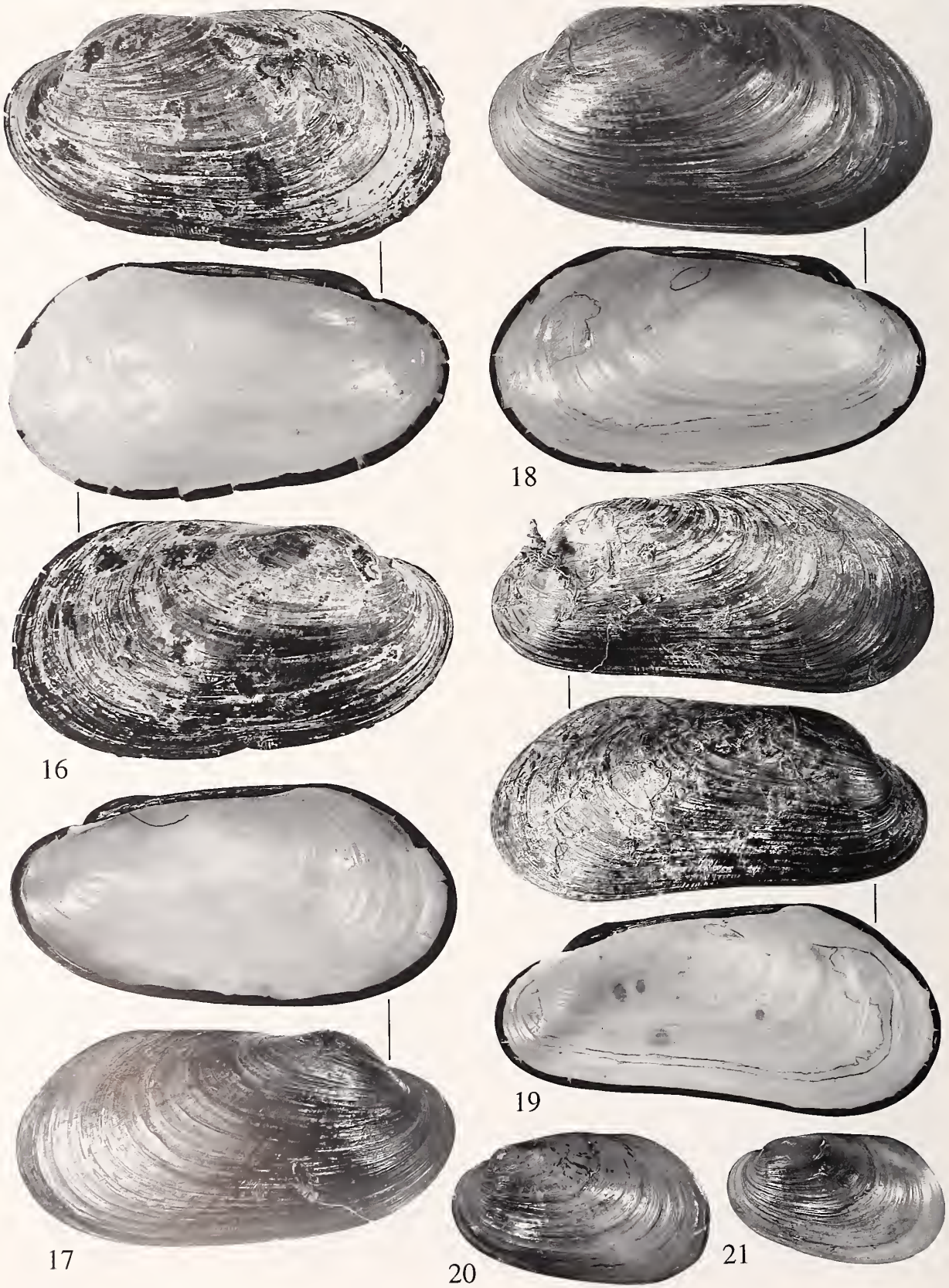
16
17
18
19
20
21

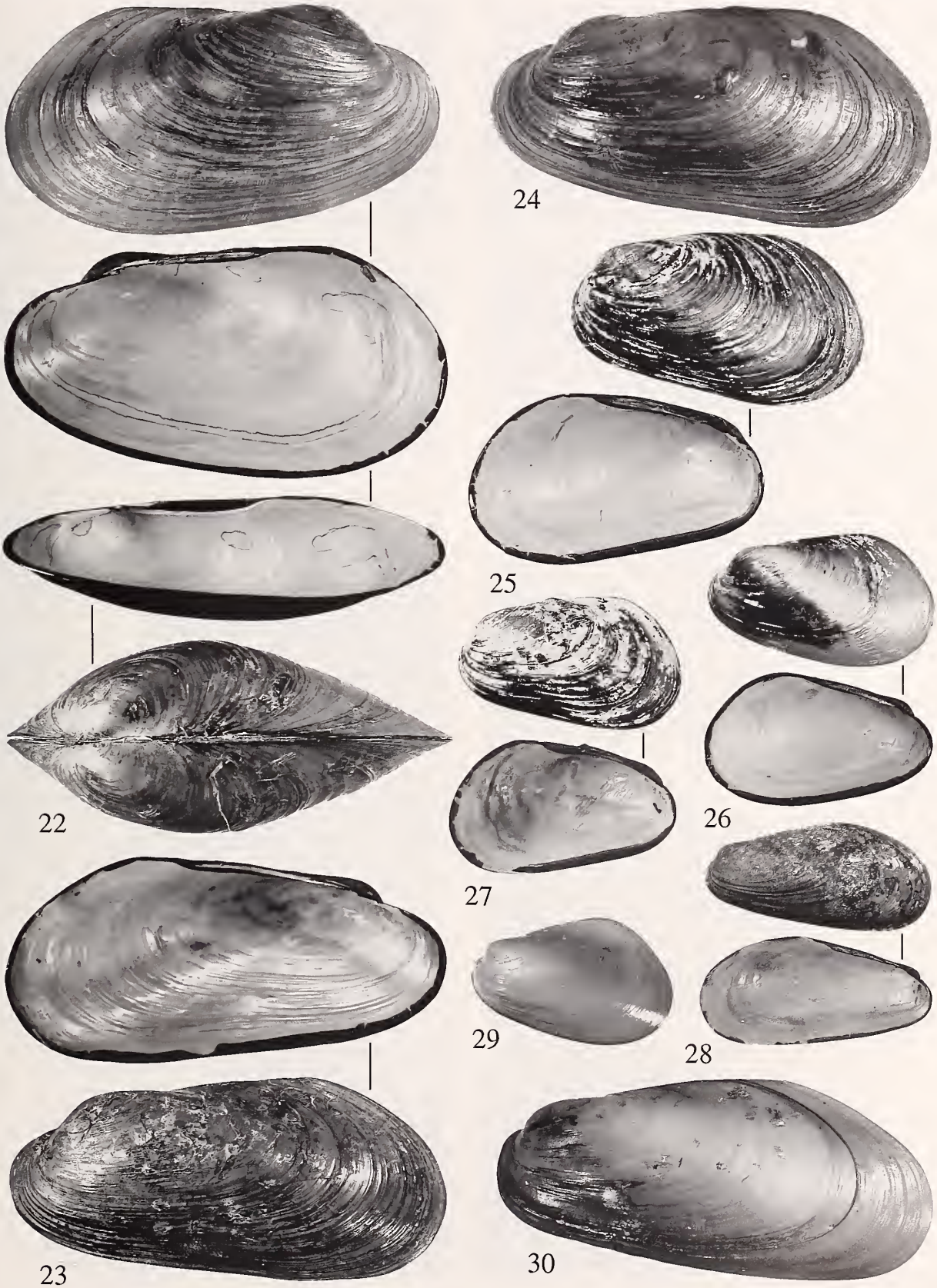
22
23
24
25
26
27
28
29
30

nies of *Bathymodiolus* ***azoricus*** are more scattered, which could be due to the presence of soft substrate. Their temperature preferences are similar to those of the mussels at Lucky Strike, ranging from about 8°C (i.e., ambient seawater temperature) to about 30°C. The mussels derive their food from intracellular symbiotic chemoautotrophic bacteria, of both sulfide-oxydizing and methanotrophic types (Fiala-Médioni et al., 1996).

On Lucky Strike hydrothermal field, many specimens of *Bathymodiolus* ***azoricus*** harbor in their pallial cavity the commensal polynoid polychaete *Branchypolynoe seepensis* Pettibone, 1986 This worm was found already in small individuals, from 33 mm length onward. In these small mussels, the polychaete is of course smaller but it can reach up to half the shell length. In the largest studied specimen of 119.3 mm, the worm was 45 mm long. In the Menez Gwen mytilids, *Branchypolynoe* were never found. A detailed ecological description of the Lucky Strike vent field is given by Van Dover et al. (1996).

Distribution: *Bathymodiolus* ***azoricus*** is only known from the Menez Gwen and Lucky Strike hydrothermal fields on the Azores Triple Junction, Mid-Atlantic Ridge.

Etymology: The name expresses the proximity of the localities of this species to the Azores archipelago.

Remarks: *Bathymodiolus* ***azoricus*** shows an extreme variability, especially in shell shape, tumidity, and length/height ratio, but also in the position of the anterior scar of the posterior byssus retractor muscle, the form of posterior end of the ligament (ending abruptly or tapering), the thickness of the shell, the anterior and posterior mantle fusion, and the size of the labial palps.

The variability of the shell is so that two "extreme" specimens of *B.* ***azoricus*** suggest two totally different species. The general shell outline can be elongate-triangular to oval-oblong or even oval-elongate, almost date-shaped. The anterior margin may be broadly or rather narrowly rounded; the postero-dorsal corner is narrowly rounded to nearly indistinct and more or less integrated into the rounded posterior margin; the postero-dorsal margin is straight to convex. Growth allometry is also variable. The surface of the shells varies from smooth and quite glossy with relatively few growth lines to more or less covered with an oxide layer and numerous byssal endplates of other mussels, with strong and dense growth lines and somewhat coarser growth stages. The ventral pallial line is straight to rather markedly curved, this mostly (not always) when the ventral margin is also concave. The shell tumidity is also considerably variable (see Figures 12 and 14); extreme forms may be even more tumid than the maximum height of the shell.

This variability in shell shape and outline is present already in medium-sized and small specimens (see Figures 25–28); the latter often have a markedly convex ventral margin or in some specimens, the margin may be already somewhat concave. Specimens from some localities are small but have a more or less adult appearance with broad (high) shell, numerous well-marked growth stages, and oxide layer.

Gonads were already present in several specimens of 30–40 mm size; the smallest specimen with clearly visible gonads measures 31.8 × 16.5 mm and is from Menez Gwen; very few gonads were evident in a specimen of 25.4 × 16.5 mm from Isabel site (Lucky Strike) and one of 28.5 × 14.6 from Menez Gwen. Many of the small specimens with gonads are more or less thick-shelled and broad with many growth marks, but not in all cases; the above-mentioned 31.8 mm specimen is smooth, rather narrow, and quite thin-shelled. A few of the larger specimens (between 60 and 76 mm) were found with very few gonads or none at all; they all have a rather thin shell. One might expect gonads in the small forms with dense growth rings and thicker shell, which can be viewed as dwarf adults that grew more slowly under less favorable ecological conditions, but the presence of gonads in small, smooth, and thin-shelled juvenile-looking specimens from Menez Gwen still needs an explanation.

The soft parts also are variable: the papilla on the valvular siphonal membrane varies from being hardly visible as a slight curve only, to being large and strongly pro-

→

Explanation of Figures 31–35

Figures 31–33. *Bathymodiolus* ***azoricus*** Cosel & Comtet sp. nov. Figure 31. Speeimen from Menez Gwen hydrothermal field, site Mogued Gwen (same speeimen as on Figure 30). Close-up view of anterior and posterior mantle fusion and posterior valvular siphonal membrane. Figure 32. Speeimen from Lucky Strike hydrothermal field, site Pagoda (PP7), 37°17.63′N, 32°16.96′W, 1629 m, DIVA 2, dive 07, shell length 56.7 mm. Close-up view of anterior and posterior mantle fusion and posterior valvular siphonal membrane. Figure 33. Speeimen from Lucky Strike hydrothermal field, same locality, shell length 59.3 mm. Close-up view of anterior and posterior mantle fusion and posterior valvular siphonal membrane. Note the different width of the "turning back" part above the anterior adductor in the three specimens. Figures 34, 35. *Bathymodiolus* sp. Figure 34. Specimen from Logatchev hydrothermal field, Irina site 14°45.10′N, 44°48.60′W, 3040 m, MIKROSMOKE, dive 21, shell length 69.1 mm. Close-up view of anterior and posterior mantle fusion and posterior valvular siphonal membrane. Figure 35. Speeimen from Logatchev hydrothermal field, Irina site 14°45.10′N, 44°48.60′W, 3040 m, MIKROSMOKE, dive 21, shell length 71.6 mm. Close-up view of anterior and posterior mantle fusion and posterior valvular siphonal membrane.


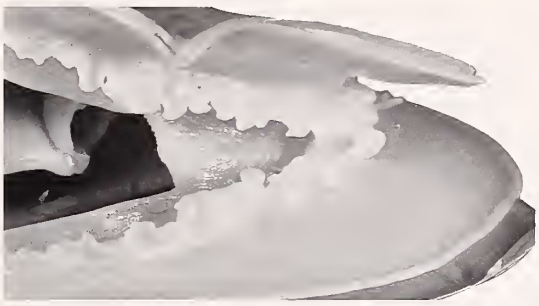

31


32

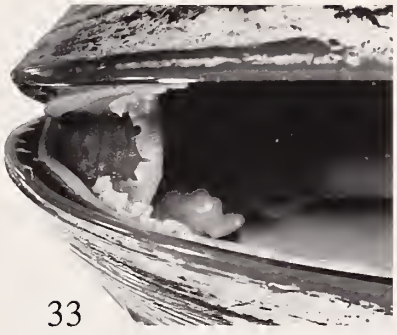


33

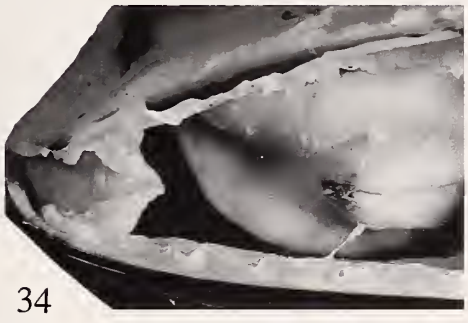
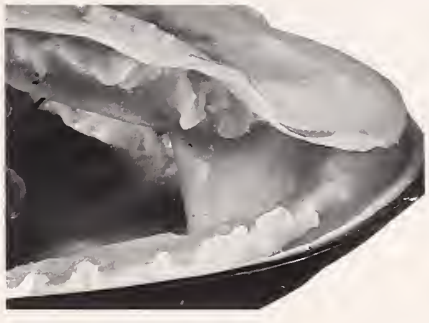

34

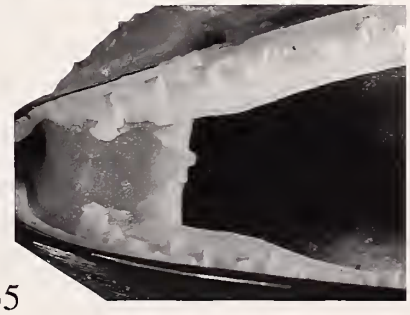


35

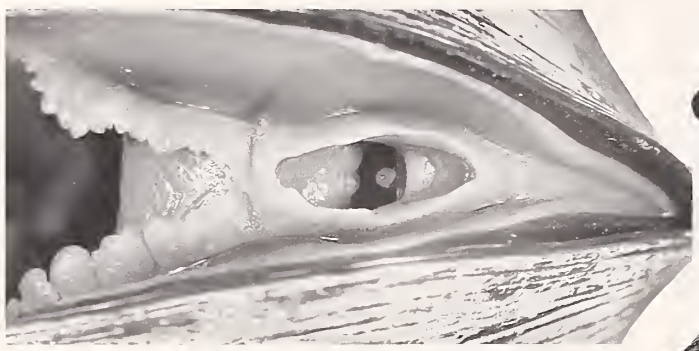

39

36

37

40

38

41

42

Explanation of Figures 36–42

Figures 36, 37. *Bathymodiolus* ***azoricus*** Cosel & Comtet, sp. nov. Figure 36. Specimen from Menez Gwen hydrothermal field, site Mogued Gwen (PP10) 37°50.56′N, 31°31.27′W, 877 m, DIVA 2, dive 12, MNHN, 85.0 mm. Ventral view showing ventral opening. One valve removed. Figure 37. Specimen from Lucky Strike hydrothermal field, site Pagoda (PP7), 37°17.63′N, 32°16.96′W, 1629 m, DIVA 2, dive 07, MNHN, 59.3 mm. Ventral view showing ventral opening. Figure 38. *Bathymodiolus sp,*. Specimen from Logatchev hydrothermal field, Irina site 14°45.10′N, 44°48.60′W, 3040 m, MIKROSMOKE, dive 20, MNHN, 81.7 mm. Ventral view showing ventral opening. One valve removed. Figures 39–42. *Bathymodiolus* ***azoricus*** Cosel & Comtet, sp. nov. Figure 39. Specimen from Lucky Strike hydrothermal field, same locality, shell length 57.5 mm. Close-up view of exhalent siphon with clearly visible anal papilla. Figure 40. Specimen from Lucky Strike hydrothermal field, site Pagoda (PP7), 37°17.63′N, 32°16.96′W, 1629 m, DIVA 2, dive 07, shell length 56.7 mm. Close-up view of exhalent siphon. Figure 41. Specimen from Menez Gwen hydrothermal field, paratype, MNHN, shell length 107.8 mm. Detail of labial palps. Figure 42. Specimen from Menez Gwen hydrothermal field, paratype, MNHN, shell length 103.0 mm. Detail of labial palps.

43

44

Explanation of Figures 43 and 44

Figures 43, 44. *Bathymodiolus* ***azoricus*** Cosel & Comtet, sp. nov., Specimen from Menez Gwen hydrothermal field, site Mogued Gwen (PP10) 37°50.56′N, 31°31.27′W, 877 m, DIVA 1, dive 13, sample 13.6. Shell length 81.1 mm. View into the siphonal cavity under two different angles. Note the anal papilla and the two tentacles on the lower transversal membrane directly under the siphonal opening (excurrent chamber) and on Figure 44 the posterior part of the incurrent chamber.

tuberant. Also the passage of the mantle edge over the anterior adductor from one valve to the other is rather variable (Figures 31–33).

All these highly variable characters are combined in nearly every sense, even within lots from the same site or dive, so that a clear delimitation of certain "morphs" is often not possible. However, in some sites, a tendency toward a certain form can be observed, especially in the site Statue of Liberty, where the specimens are exceptionally slender for a Lucky Strike population (Figures 6, 7).

Differences are more clear and seem to be more stable between the specimens of the two hydrothermal fields, Lucky Strike and Menez Gwen, which have a horizontal distance of about 60 km and a depth difference of about 800 m. Menez Gwen mussels have the umbos still somewhat more forward (see Figures 1–5) than those from Lucky Strike (for more details, see Biometry).

This variability is probably mainly due to abiotic ecological factors such as degree of nutrition (availability of nutrients), degree of venting activity (which can change rapidly), physico-chemical conditions, composition and temperature of the water, etc., but also to biotic factors, e.g., population density and competition. All these factors determine growth speed and growth allometry. The more tumid specimens with dense growth lines certainly did not have as favorable conditions as those with a smooth surface, sharp margins, and no incrustations. These specimens obviously grew faster and were less disturbed. Some characters might perhaps also be related to genetic factors. In some sites (e.g., Menez Gwen) there is a tendency toward a certain homogeneity, but also there a few specimens of other "morphs" were present in a sample. In other sites, however, all morphs occurred together.

Two rather stable characters, however, which distinguish the shells of *B.* ***azoricus*** from *B. puteoserpentis,* are the position of the anterior byssus retractor scar and the position of the umbos relative to shell length. In *B. puteoserpentis,* the anterior byssus retractor scar is situated on the anterior part of the umbonal cavity in front of the umbos, whereas in the new species, the byssus retractor inserts more posterior within the umbonal cavity, normally directly under the umbos. *B.* ***azoricus*** is generally somewhat more elongate, and the umbos are always placed more forward than in *B. puteoserpentis,* at one-tenth to one-twelfth of shell length or more as opposed to one-seventh in *B. puteoserpentis.* Among the known vent mussels, only *B. platifrons* Hashimoto & Okutani, 1994, has similar almost terminal umbos.

We conclude that all "morphs" belong to a single very variable species and that even genetic differences between the sites (if present) are too small to warrant separation.

Bathymodiolus sp. aff. *B. puteoserpentis*
(Figures 16–24, 34, 35, 38, 53–56, 61, 63–67)

Description: Shell large, up to 123 mm long, thin but rather solid, modioliform-oval, considerably variable in outline, inflated, equivalve. Juvenile specimens in general somewhat shorter and more oval than adults but also already quite variable. Beaks subterminal. Anterior margin rather broadly rounded; ventral margin straight to slightly convex, in large and fully grown specimens often slightly concave in middle. Postero-ventral margin broadly rounded, postero-dorsal margin slightly convex to almost straight; postero-dorsal corner rather broadly to very broadly rounded; ligament plate arched, often more in its anterior half. Exterior with well-developed and strong, irregular growth lines and growth waves, which are well reflected on inside. In juveniles and half-grown specimens, weak and fine radial sculpture mostly visible in middle part of ventral half of valve as rather dense, irregular radial wrinkles (see Figure 19); occasionally also faint, narrow radial lines or waves on posterior slope (see Figure 17). Some faint radial structure also visible on inside of valves within shell material but not sculpturally reflected on the internal surface like growth lines. Umbos broad, very flattened.

Shell without periostracum dull whitish; interior nacreous white.

Periostracum strong, brown with a slight tendency toward olive, in umbonal and postero-dorsal region lighter brown, somewhat glossy, with no periostracal hairs; however, byssal endplates of other specimens always scattered over whole valve.

Hinge edentulous, anterior hinge margin, however, slightly protruding toward ventral. Ligament opisthodetic, strong, extending over almost whole postero-dorsal margin to postero-dorsal corner. Subligamental shell ridge very faint from under umbos to middle of ligament, then becoming obsolete; under beaks visible only in ventral view and not in lateral view. Anterior adductor scar long-oval, arched, situated in front of umbo. Posterior adductor scar rounded-trapezoid, united with posterior scar of posterior foot and byssus retractor muscle. Anterior scar of same muscle separated and situated under ligament, at slightly behind two-thirds of its length (Figure 19). In smaller specimens, this scar is more backward (Figure 22) and in very small (35 mm and smaller) mussels, it is situated just behind ligament's end. Anterior byssus retractor muscle scar on anterior part of umbonal cavity just in front of beaks, visible only in posterior and ventral view but not in lateral view of interior. Pallial line ventrally straight, in large specimens often slightly concave when ventral margin is also concave.

Larval shell 390–400 μm long and 380 μm high (Figures 53–56). Protoconch I 120 μm long, with irregular surface and well separated from Protoconch II, which indicates a long planktonic larval phase. Surface of Protoconch II with very fine, densely spaced and regular concentric grooves which may not always be visible.

Animal with large ctenidia which are about three-fourths of shell length and cover entire visceral mass, each demibranch with descending and shorter ascending lamellae. Outer demibranch anteriorly slightly shorter than inner demibranch. Ascending lamellae of outer and inner demibranchs anteriorly fused to mantle and to visceral mass, respectively, for very short distance; more posteriorly gills entirely free from fusion. No muscular longitudinal ridges on mantle and visceral mass where dorsal edges of ascending lamellae attach. Connection bars between free edges and gill axes absent. Ventral edge with shallow food groove. Outer surface of ascending lamellae of both demibranchs with folds just below free edges and parallel to them. Filaments wide, fleshy, connected with each other by "plaquettes" and "racquets" (Le Pennec & Hily, 1984) on ventral and lateral sides, respectively. Approximately each fourth to seventh filament with septum reaching to half of gill height and connecting lamellae. In juvenile specimens, ascending lamellae of demibranchs much shorter than descending lamellae; in adult specimens, lamellae almost equal-sized.

Mantle thin, except for heavily thickened muscular margin and vascularized anterior region. Mantle edges with three folds; posteriorly, inner mantle folds fused dorsally above exhalent siphon and between exhalent siphon and combined inhalent aperture and pedal gape, forming short, narrow, and rather strong valvular siphonal mem-

→

Explanation of Figures 45–52

Figures 45–52. *Bathymodiolus* ***azoricus*** Cosel & Comtet, sp. nov. Larval shells. Figures 45–48. Specimens from Menez Gwen hydrothermal field, 37°50.54′N, 31°31.30′W, DIVA 2, dive 11. Figure 45. Juvenile specimen. Scale bar: 200 μm. Figure 46. Close-up view of Protoconch II of the same specimen. Scale bar: 100 μm. Figure 47. Protoconch II of another specimen. Scale bar: 100 μm. Figure 48. Protoconch I of another specimen. Scale bar: 20 μm. Figures 49–52. Specimens from Lucky Strike hydrothermal field, site Eiffel Tower, 37°17.32′N, 32°16.52′W, 1685 m, DIVA 2, dive 10. Figure 49. Juvenile specimen. Scale bar: 200 μm. Figure 50. Another specimen showing Protoconchs I and II. Scale bar: 100 μm. Figure 51. Close-up view of Protoconch I of the same specimen. Scale bar: 10 μm. Figure 52. Protoconch II of another specimen, showing the more or less widely spaced concentric striae. Scale bar: 100 μm.

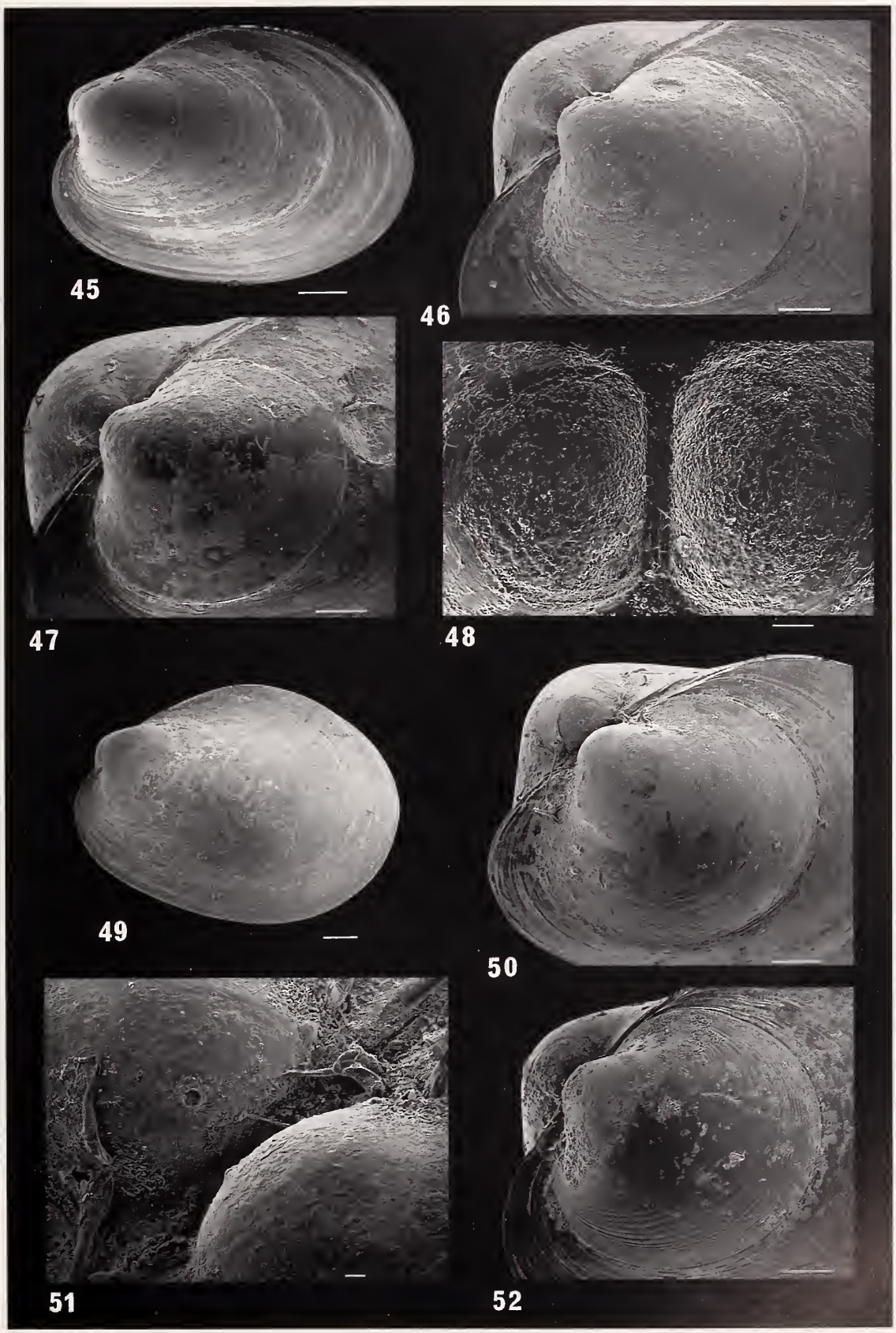
45
46
47
48
49
50
51
52

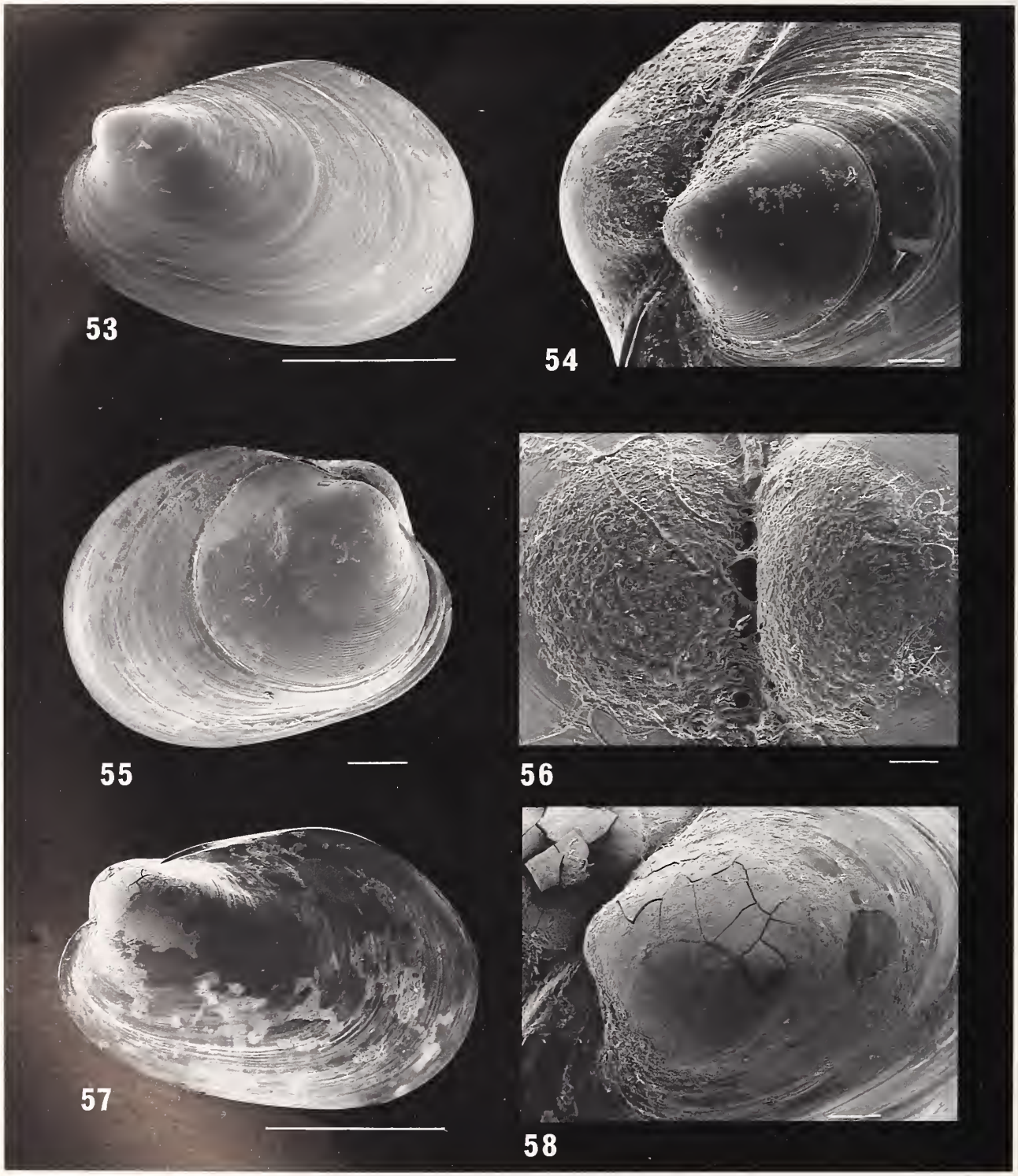

Explanation of Figures 53–58

Figures 53–56. *Bathymodiolus* sp.. Specimens from Logatchev hydrothermal field, Irina site, 14°45.10′N, 44°48.60′W, 3063 m, MIKROSMOKE dive 20. Figure 53. Juvenile specimen. Scale bar: 1 mm. Figure 54. Close-up view of Protoconch II of the same specimen. Scale bar: 100 μm. Figure 55. Ultra-juvenile specimen with well-distinguished Protoconch I and Protoconch II. Scale bar: 100 μm. Figure 56. Close-up view of Protoconch I of the

brane which reaches from siphonal opening to posteroventral corner and bears a small papilla. Anteriorly, inner mantle folds fused for very short distance underneath anterior adductor muscle. Mantle folds passing from ventrally over adductor muscle up- and foreward along anterior margin, then folding down- and backward to pass again lower end of anterior adductor muscle toward ventral margin. Inner mantle folds frilled over all their length (Figure 38). Pallial muscles and siphonal retractors strong. Exhalent siphon short, inner aperture of it occluded by thin internal diaphragm with narrow horizontal slit. Muscular fold around slit which regulates aperture size. Two small, flattened tentacles directed toward anus situated under slit. As a branchial septum and a fusion of the gills with each other are absent, division of mantle cavity into a ventral incurrent and a dorsal excurrent chamber is not complete.

Foot thick, broad, flattened, tapering toward end, with ventral byssal groove three-fourths the length of foot. Anterior byssus retractor moderately long, strong, divided into three small blocks at about half its length. Posterior byssus retractor consisting of two strong, diverging muscle bundles of approximately equal width as anterior byssus retractor and having common base at base of byssus. Anterior bundle about two times shorter than posterior bundle and arising steeply toward attachment point on shell. Posterior bundle divided into two parallel bundles over all its length and passing at low angle to longitudinal shell axis. Posterior pedal retractor slightly more slender than other muscle bundles, arising from base of foot anterior to origin of posterior byssus retractors, passing outer side of anterior retractor toward anterior bundle of posterior byssus retractor. Posterior pedal retractors slightly asymmetrical, right one divided into two bundles at about half its length, both bundles inserting on inner and anterior sides of anterior bundles of posterior retractors. Left pedal retractor divided into two bundles over all its length, one bundle inserting on outer side of anterior bundle of posterior retractor at half its length, and other bundle inserting on inner side of anterior bundle.

Labial palps narrow, triangular, short but stout, strongly ridged on inner surfaces, anterior palps slightly smaller than posterior ones. Labial palp suspensor muscles present. From lateral sides of mouth between palps narrow fold running to base of gills. Labial palps of juveniles much shorter and sometimes lacking ridges.

Mouth transverse, slitlike, opening into short, thin-walled esophagus. Esophagus entrance at anterior end of stomach surrounded by dark digestive diverticula. Inner

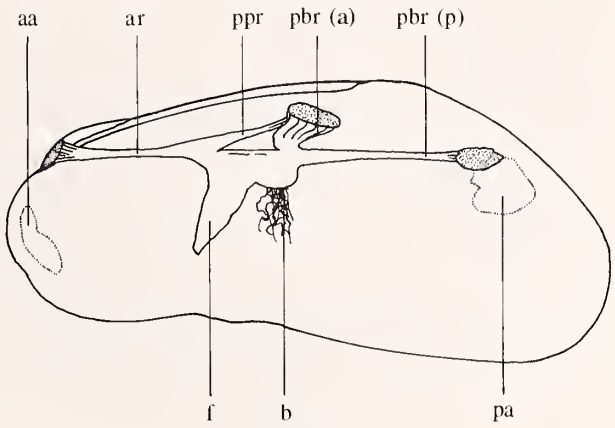

Figure 59

Sketch of foot-byssus retractor muscle complex of *Bathymodiolus azoricus* Cosel & Comtet, sp. nov., and its position in the shell (separate slender strand of anterior retractor serving as support for labial palps not drawn); specimen from Menez Gwen DIVA 2, Pl. 13; shell size 98.5 mm; aa, anterior adductor; ar, anterior retractor; ppr, posterior pedal retractor; pbr (p), posterior byssus retractor, posterior bundle; pbr (a), posterior byssus retractor, anterior bundle; pa, posterior adductor; f, foot; b, byssus.

surface of esophagus near its entrance into stomach bearing longitudinal ridges. Stomach (Figure 66) thin-walled, small, elongate, divided into a round anterior, and a more conspicuous posterior chamber. Major typhlosole arising from conjoined style sac and midgut, passing forward along floor of posterior chamber of stomach and terminating in shallow depression of floor of anterior chamber, possibly corresponding to food-sorting caecum. Gastric shield on antero-dorsal wall on left side of posterior chamber. Altogether, 11 ducts of digestive diverticula open into stomach. Posterior chamber with six openings. Three ducts of left side open into shallow depression below gastric shield, corresponding to left pouch. Small grooves leading from every opening of ducts and joining to form beginning of intestinal groove. Intestinal groove following major typhlosole, turning right and running along right side of major typhlosole into midgut. To right of intestinal groove and parallel to it, shallow groove running on lateral side of posterior chamber. Three ducts of digestive diverticula of right side opening along side of groove. Five ducts of digestive diverticula opening in anterior chamber near esophagus entrance—two openings from left side and three on floor and from right side. Crystal style present as amorphic mass. Arrangement of

←

same specimen. Scale bar: 20 μm. Figures 57, 58. *Bathymodiolus puteoserpentis* Cosel, Métivier & Hashimoto, 1994 (for comparison). Snake Pit hydrothermal field, Elan site, 23°22′N, 47°57′W, 3520 m, MIKROSMOKE dive 14. Figure 57. Juvenile specimen. Scale bar: 1 mm. Figure 58. Close-up view of Protoconch II, firmly covered by oxide layer but limits more or less visible. Scale bar: 100 μm.

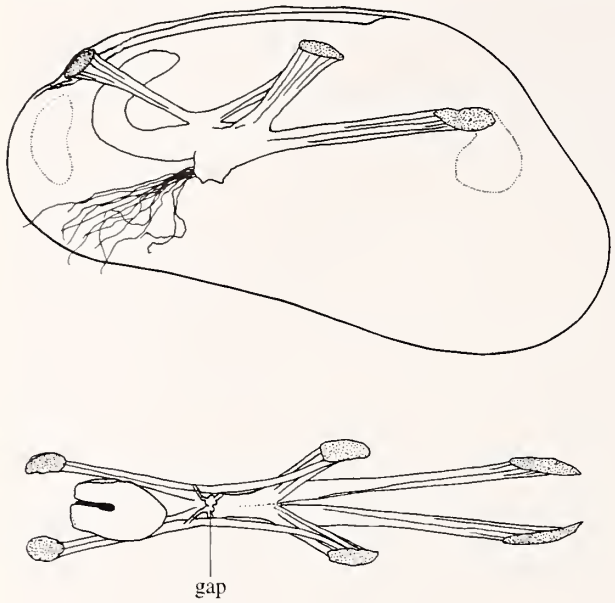

Figure 60

Sketch of foot-byssus retractor muscle complex of *Bathymodiolus azoricus* Cosel & Comtet, sp. nov.; specimen from Lucky Strike, DIVA 2, Pl 07, Pagoda. Shell illustrated on Figure 8, size 91.1 mm. Above, lateral view of the complex and its position in the shell (separate slender strand of anterior retractor serving as support for labial palps not drawn); below, ventral view (slightly enlarged as against the lateral view); gap, pedal ganglion.

openings of digestive diverticula to anterior stomach chamber may be variable. In very large specimens, inner surface of stomach more smooth and plain.

Midgut leaving the postero-ventral end of stomach and running for short distance posteriorly down mid-line, then entering pericardium and making very short counterclockwise recurrent loop under ventricle before entering it ventrally and slightly anterior to auricular ostia. Rectum running directly down mid-line toward posterior and ending in a papillate anus on posterior surface of posterior adductor muscle. Dorsal wall of anus longer than its ventral wall, lateral sides bearing flattened ridges running to posterior point of attachment of gills axis to visceral mass. Shape of outgrowths of dorsal wall of anus variable. Examined stomach contained mytilid juveniles, sand, and mucuslike material; the rectum contained sand.

Heart three-chambered; ventricle rather large (in some preserved specimens), somewhat triangular, muscular, auricles very large, fused together posteriorly and with protrusions between bundles of posterior byssus retractors.

Kidney situated on each side of body below pericardium close to longitudinal vein, consisting of a thin-walled lobulate duct. Renopericardial apertures located in antero-lateral extremities of pericardium.

Sexes separate, gonads enclosing digestive diverticula and in large specimens extending into mantle. Genital apertures located at tips of small papillae in excurrent chambers near byssus.

Selected measurements (length, height, tumidity) with length–height ratios:

123.2 × 57.0 × 46.2 mm	Pl 21	2.2
120.7 × 54.4 × 46.6 mm	Pl 20	2.2
120.3 × 56.1 × 45.4 mm	Pl 21	2.1
94.7 × 49.6 × 39.8 mm	Pl 20	1.9
83.2 × 41.2 × 33.2 mm	Pl 21	2.0
81.9 × 39.8 × 31.1 mm	Pl 20	2.1
89.2 × 43.1 × 38.9 mm	*Akademik Mstislav Keldysch*	2.1
74.1 × 37.1 × 33.6 mm	*Prof. Logatchev*	2.0
72.7 × 36.7 × 30.7 mm	Pl 21	2.0
71.7 × 36.4 × 28.4 mm	Pl 20	2.0
71.4 × 38.4 × 30.6 mm	Pl 20	1.9
71.4 × 35.1 × 29.0 mm	Pl 20	2.0
68.0 × 33.4 × 31.4 mm	*Akademik Mstislav Keldysch*	2.0
69.3 × 35.7 × 32.2 mm	Pl 21	1.9
65.1 × 34.3 × 26.1 mm	Pl 21	1.9
61.5 × 32.5 × 27.3 mm	*Akademik Mstislav Keldysch*	1.9
54.5 × 30.6 × 23.7 mm	Pl 21	1.8
54.1 × 29.2 × 20.2 mm	Pl 20	1.9
53.5 × 31.2 × 24.7 mm	Pl 21	1.7
47.5 × 27.8 × 18.8 mm	Pl 20	1.7
41.2 × 24.2 × 15.2 mm	Pl 20	1.7
37.8 × 22.4 × 16.0 mm	Pl 20	1.7
31.7 × 19.4 × 13.2 mm	Pl 20	1.6
22.5 × 14.8 × 9.1 mm	*Akademik Mstislav Keldysch*	1.5
19.2 × 12.2 × 8.1 mm	*Akademik Mstislav Keldysch*	1.6
19.0 × 13.9 × 6.9 mm	*Akademik Mstislav Keldysch*	1.4
14.4 × 8.4 × 5.3 mm	*Akademik Mstislav Keldysch*	1.7
12.2 × 7.9 × 4.8 mm	*Akademik Mstislav Keldysch*	1.5
11.5 × 8.0 × 4.5 mm	*Akademik Mstislav Keldysch*	1.4
11.3 × 7.5 × 4.3 mm	*Akademik Mstislav Keldysch*	1.5
11.2 × 7.3 × 4.2 mm	*Akademik Mstislav Keldysch*	1.5
9.1 × 5.9 × 3.5 mm	*Akademik Mstislav Keldysch*	1.5
8.9 × 5.9 × 3.6 mm	*Akademik Mstislav Keldysch*	1.5
8.7 × 5.3 × 3.2 mm	*Akademik Mstislav Keldysch*	1.6
8.3 × 5.6 × 3.6 mm	*Akademik Mstislav Keldysch*	1.5

Material examined: Mid-Atlantic Ridge, 14°45′N, 44°58′W, Logachev hydrothermal field, cruise 35, R/V *Akademik Mstislav Keldysch,* sta. 3452, 16 spm. (among

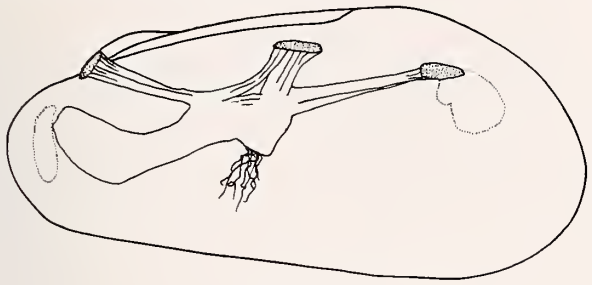

Figure 61

Sketch of foot-byssus retractor muscle complex of *Bathymodiolus* sp. from Logatchev and its position in the shell (separate slender strand of anterior retractor serving as support for labial palps not drawn); specimen from Pl. 21, shell length 120.3 mm. For explanation, see Figure 59.

them 12 juv.), 1 sh., taken by submersible Mir-2, dive 4/171, E.S. Chernjev, observer, 23 February 1995, ZMM Moscow. Irina site, 14°45, 10′N, 44°48.60′W, 3063 m, MICROSMOKE, dive 20, D. Prieur, observer, 5 December 1995, 11 spm., 20 juv. spm.; same locality, 3040 m, dive 21, Y. Fouquet, observer, 6 December 1995, 7 spm.; same locality, LOGATCHEV-7 cruise, R/V *Professor Logatchev*, 1 empty shell taken by TV equipped grab, July 1994, MNHN.

Biotope: The animal community of Logatchev hydrothermal field is dominated, in terms of biomass, by *Bathymodiolus* sp., which forms dense aggregations slightly below the zone of shimmering water (Gebruk et al., 1997). A commensal polynoid polychaete, which remains to be identified, was found in the mantle cavity of *Bathymodiolus* sp, but it occurs with a lower frequency than *Branchypolynoe seepensis* in *Bathymodiolus* ***azoricus.*** In 23 examined specimens, only four were found to host the polychaete, and the worm was also smaller in relation to shell length than in ***B. azoricus.*** An ecological description of the Logatchev field is given in Gebruk et al. (1997).

Distribution: Mid-Atlantic Ridge, known only from the Logatchev hydrothermal field, 14°45′N, 44°58′W, 2930–3063 m.

Remarks: The mussels from the Logatchev field population are extremely close to *B. puteoserpentis,* and we do not find any really stable distinguishing character which would allow us to describe this *Bathymodiolus* as a new species separate from the Snake Pit mussels; however, there are some subtle differences in morphology

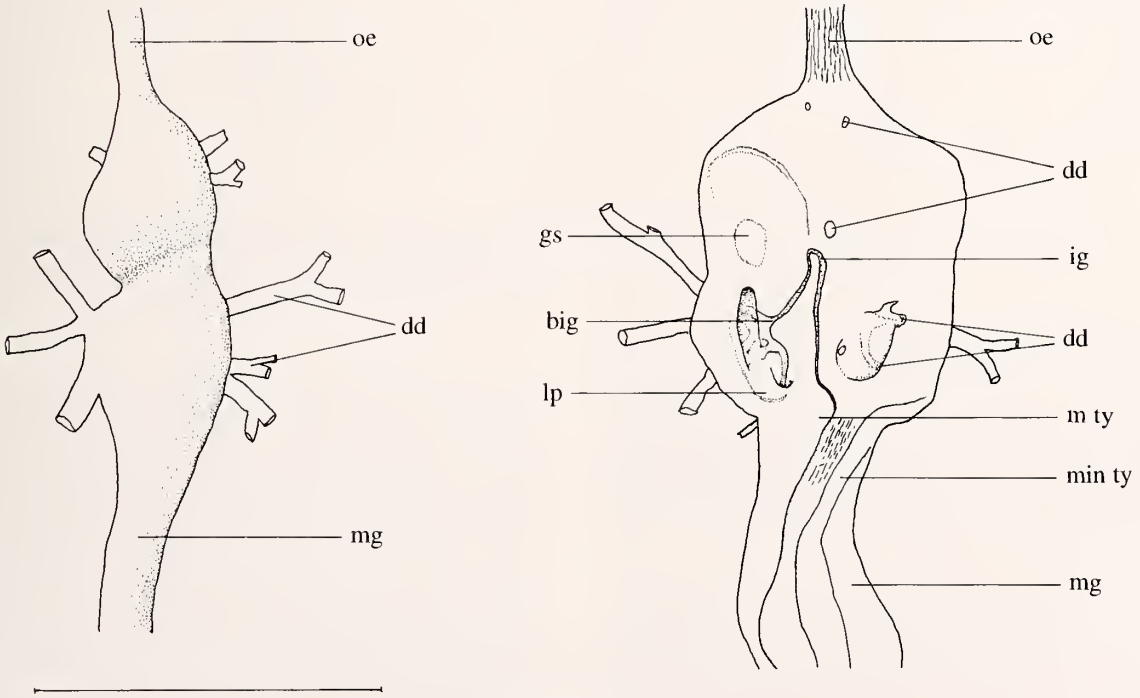

Figure 62

Stomach of *Bathymodiolus* ***azoricus*** Cosel & Comtet, sp. nov. from Lucky Strike. Halfschematic drawings from the same specimen as on Figure 60. Left, general view: above, anterior chamber; below, posterior chamber; dd, digestive diverticula ducts. Right, stomach opened dorsally; oe, esophagus; dd, digestive diverticula ducts (entrances); ig, intestinal groove; gs, gastric shield; big, beginning of intestinal groove; lp, left pouch; m ty, major typhlosole; min ty, minor typhlosole; mg, midgut. Scale: 1 cm.

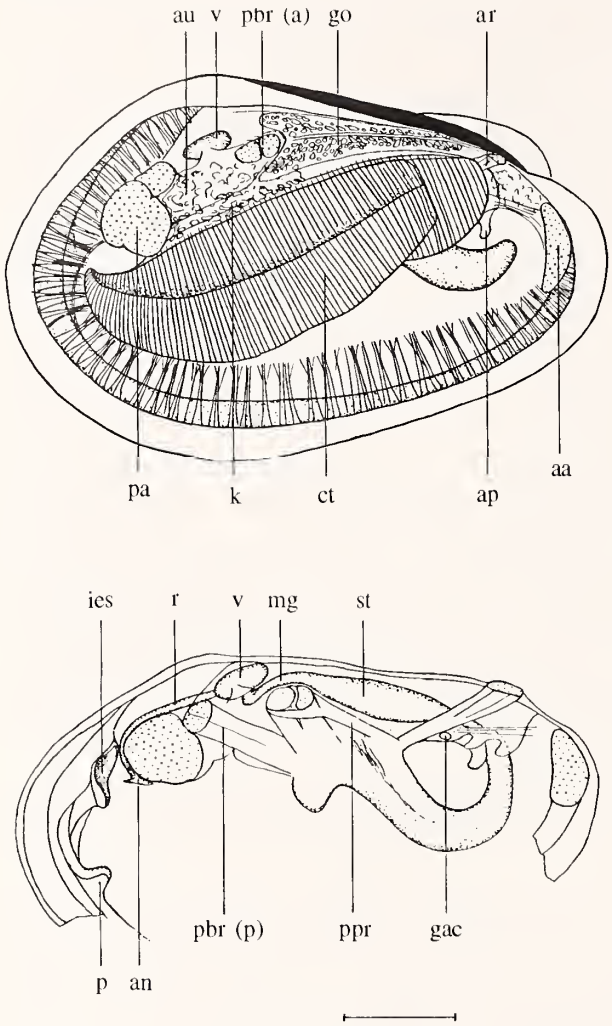

Figure 63

Bathymodiolus sp. Above, specimen of Figure 16, general view of soft parts. pa, posterior adductor; pbr (p), posterior byssus retractor, posterior bundle; pbr (a), posterior byssus retractor, anterior bundle; v, ventricle; au, auricle; go, gonads; k, kidney; ct, ctenidia; ar, anterior retractor; ap, anterior labial palps; aa, anterior adductor; f, foot. Below, another specimen, right mantle lobe and ctenidia removed. p, papilla of siphonal membrane; ies, inner aperture of exhalent siphon; r, rectum; mg, midgut; ppr, posterior pedal retractor; st, stomach; gac, cerebral ganglion. Scale: 1 cm.

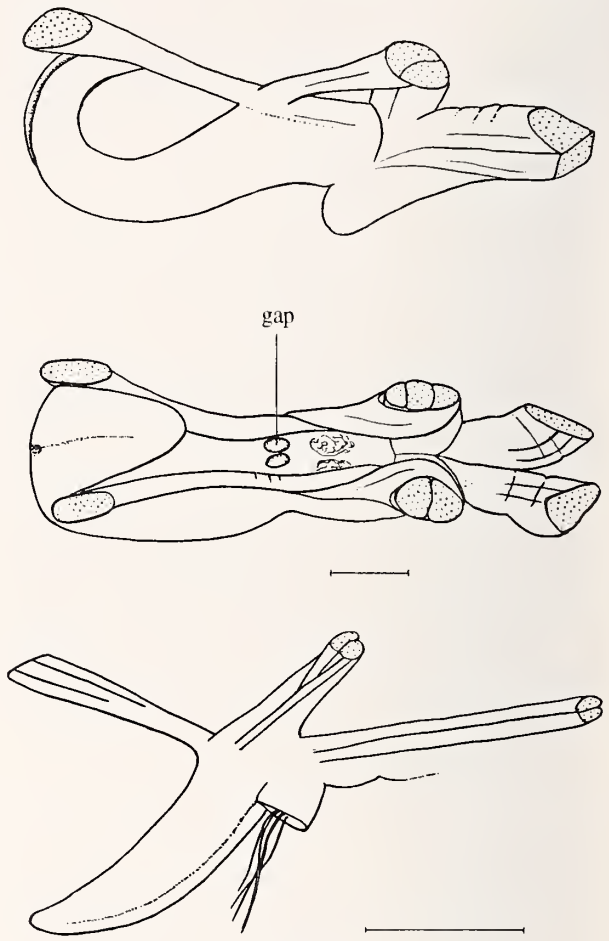

Figure 64

Bathymodiolus sp., foot-byssus retractor muscle complex. Above and middle: a juvenile specimen, lateral and dorsal view; below: holotype, lateral view; gap, pedal ganglion; for other explanations, see Figure 59. Scale: A–B: 1 mm; C: 1 cm.

(this paper) and genetics (Jollivet & Comtet, unpublished results). The mussel populations of both hydrothermal vent fields show a considerable variability in shell outline, and they overlap largely in their degree of variability. *Bathymodiolus* sp. differs from *B. puteoserpentis* from Snake Pit in its generally slightly thinner shell, which in very large specimens appears somewhat more elongate; however, in *B. puteoserpentis* rather elongate specimens were also found. The color of the periostracum tends more toward olive green in *Bathymodiolus* sp., and some specimens in coloration and surface with growth lines and growth waves, as well as in shell thickness, resemble freshwater mussels like *Anodonta,* whereas *B. puteoserpentis* is more chestnut brown. The irregular radial wrinkles on the middle part of the ventral slope are present in both species, but in *B. puteoserpentis* they are often less pronounced and also often hidden by the layer of oxide. The protoconch II in both populations is approximately the same size. The most important distinctive feature is the intestine, which in the observed *Bathymodiolus* sp. has a small counterclockwise recurrent loop under the ventricle, but in *B. puteoserpentis* the intestine changes its direction twice in an S-like manner in more or less the same plane. However, the shape of the intestine coiling seems to be variable within the same species or populations of both Snake Pit and Logatchev (and also in other species, unpublished observation in *B. brevior* Cosel, Mé-

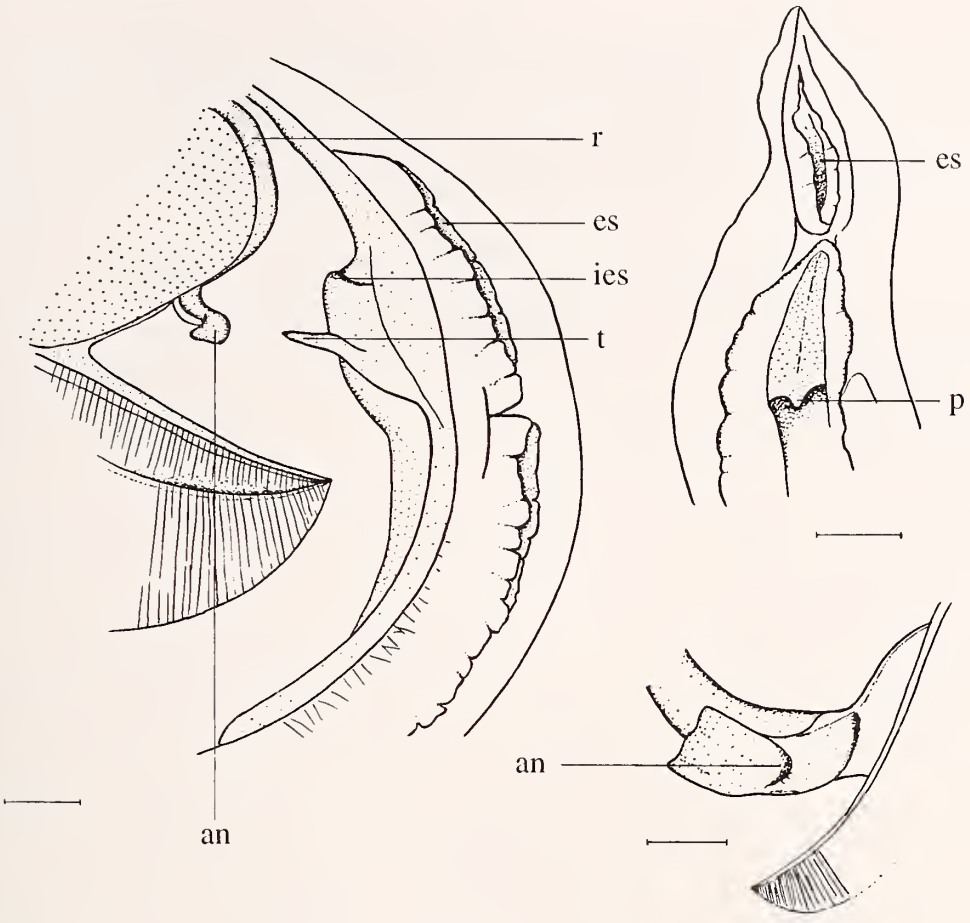

Figure 65

Bathymodiolus sp. Left, posterior part of soft parts, lateral view; upper right, exhalent siphon, posterior view; lower right, anus. r, rectum; an, anus; ies, inner aperture of exhalent siphon; es, exhalent siphon; p, papilla of siphonal membrane; t, tentacle of the lower transversal membrane. Scale: left: 2 mm; right: 1 mm.

tivier & Hashimoto, 1994), and with the few examined specimens of both populations at hand, we cannot for the moment use this character as the only one to separate the Logatchev population on species level. On the other hand, the slight morphological differences, as well as preliminary results of the current genetic research, do not permit us to identify the Logatchev mussel entirely with *B. puteoserpentis*.

Bathymodiolus ***azoricus*** is easily distinguished by the different shell outline, the almost terminal umbones with a very short anterior part, the considerably larger protoconch II, and the relationship of protoconch I/protoconch II. The protoconch I of *B.* ***azoricus*** is, in contrast to protoconch II, slightly smaller than in *Bathymodiolus* sp. A genetic study, which is currently in progress by the second author, will finally determine the genetic distances between the mussels from Logatchev, Snake Pit, and the Azores Triple Junction; these results and examination of further material will also clarify the status of the Logatchev mussel.

Both *B.* ***azoricus*** and *Bathymodiolus* sp. are distinguished from *B. thermophilus* by the lack of a ventral mantle fusion, a more complicated stomach with left pouch, a coiled intestine, the absence of a lateral muscular ridge on the mantle lobes and visceral mass, and the absence of connecting bars between the free edges of the demibranchs and the gill axes. In comparison with *B. thermophilus,* the two species here treated are less specialized. They have a much closer affinity to other *Bathymodiolus*-like species from hydrothermal vents, e.g., *B. puteoserpentis* and an undescribed *Bathymodiolus* from the Mariana back-arc basin (Craddock et al., 1995). Apart from the intestine coiling, our two species do not differ from other vent *Bathymodiolus*-like mytilids in anatomical characters used by Craddock et al., 1995. See Table 1 for a comparison of features.

Table 1

Comparison of some features of *B. thermophilus* and MAR *Bathymodiolus*.

	B. thermophilus (from 13°N)	*B. azoricus*	*Bathymodiolus* sp. (Logatchev)	*B. puteoserpentis*
General shell form:	moderately elongate	more or less elongate	moderately elongate to stout	somewhat stout to moderately elongate
Tumidity:	more or less compressed	compressed to tumid	moderately tumid	moderately tumid
Shell:	thin but solid	thin to rather thick	thin but solid	thin but solid
Position of umbos:	subterminal	almost terminal	subterminal	subterminal
Position of anterior part of posterior byssus retractor muscle scar:	under the end of the ligament	under the end of ligament or more forward	at 2/3 of the ligament but variable	under posterior third of ligament, near the end
Position of anterior byssus retractor scar in the umbonal cavity:	slightly behind the umbos	under the umbos	under and in front of the umbos	under and in front of the umbos
Ventral pallial line:	markedly deflected	straight to deflected	straight	nearly straight
Intestine:	straight	counterclockwise loop	counterclockwise loop	changes direction twice
Mantle lobes on anterior half of ventral side:	fused	separate	separate	separate
Valvular siphonal membrane:	long and thin	short, narrow	short	short
Papilla in valv.s.memb:	present	present but variable	present, small	present
Muscular longitudinal ridge on mantle lobes and visceral mass:	present	absent	absent	absent
Posterior end of ligament:	tapering	abrupt to tapering	abrupt	abrupt to slightly tapering
Subligamental shell ridge:	strong and angular	obsolete from umbo to middle then missing	faint to obsolete	faint to obsolete

BIOMETRY

Length–Height Relationships

Figures 70 and 71 show the allometric relationships between shell height and length for the three species. Allometric curves were fitted following the allometric model of Teissier (1948), of the form $H = aL^b$, using Microsoft Excel 5.0. For the three species treated, these curves indicate that length increases faster than height, traducing an elongation of the shell during growth. These results confirm those given by Comtet (1994) from samples collected on the sites Sintra and Eiffel Tower during the LUCKY STRIKE 93 cruise. For *Bathymodiolus* ***azoricus*** (Figure 70), the results indicate a great intersite variability in shell shape in individuals larger than 20 mm. The allometric relationship for the Menez Gwen population is in the range of those for Lucky Strike, indicating that mussels of both hydrothermal fields cannot be distinguished by biometrical characteristics. *Bathymodiolus* sp. and *B. puteoserpentis* have a similar shape in the observed length range (Figure 71).

For the statistical comparisons, length/height ratio was used as an index of shape (Cosel et al., 1994). Comparisons were made on individuals larger than 20 mm.

A one-way analysis of variance (ANOVA) was run to compare length/height ratios in *Bathymodiolus* ***azoricus*** from different sites of the Lucky Strike and Menez Gwen hydrothermal fields, in three different length classes (20–50 mm; 50–70 mm; larger than 70 mm) (Table 2). Due to the small sample size, the site PP5 was not included in the comparison. For the same reason, only four sites were considered for individuals larger than 70 mm. In each size class, length/height ratios are significantly different ($P = 0.0001$) (Table 2). However, pairwise comparisons using the Fisher PLSD test show no significant difference (significance level 95%) between the sites Isabel, Pagoda, and Sintra, in the three size classes.

	Fisher PLSD		
	$20 \leq L$ (mm) < 50	$50 \leq L$ (mm) < 70	$70 \leq L$ (mm)
Isabel vs. Pagoda	0.047	0.050	0.054
Isabel vs. Sintra	0.051	0.050	—
Pagoda vs. Sintra	0.041	0.049	—

All other pairwise comparisons show significant differences (significance level 95%).

Table 2

Bathymodiolus ***azoricus.*** Length/height ratios calculated for each site of the Menez Gwen and Lucky Strike vent fields, in three length classes. n: sample size.

	Mean	Standard	n	ANOVA
$20 \leq L$ (mm) < 50				
Isabel	1.756	0.136	45	
Pagoda	1.781	0.120	108	
Eiffel Tower	1.833	0.147	535	$P = 0.0001$
Sintra	1.763	0.133	67	
Statue of Liberty	2.051	0.130	592	
Menez Gwen	2.009	0.122	83	
$50 \leq L$ (mm) < 70				
Isabel	1.987	0.119	46	
Pagoda	1.974	0.099	51	
Eiffel Tower	2.036	0.133	151	$P = 0.0001$
Sintra	1.989	0.102	51	
Statue of Liberty	2.289	0.144	47	
Menez Gwen	2.162	0.126	114	
$70 \leq L$ (mm)				
Isabel	2.080	0.099	42	
Pagoda	2.110	0.109	63	$P = 0.0001$
Eiffel Tower	2.153	0.165	116	
Menez Gwen	2.286	0.130	89	

Table 3

Length/height ratios in *Bathymodiolus* ***azoricus,*** *Bathymodiolus* sp. (Logatchev) and *B. puteoserpentis* from different localities on the MAR, after the subsampling procedure. n: subsample size.

	Range	Mean	Standard	n
Bathymodiolus ***azoricus***				
Eiffel Tower	1.387–2.619	2.057	0.201	100
Isabel	1.518–2.343	1.900	0.199	80
Pagoda	1.595–2.321	1.973	0.163	102
PP5	1.674–2.374	2.036	0.200	62
Sintra	1.491–2.419	1.909	0.199	74
Statue of Liberty	1.832–2.439	2.165	0.156	52
Menez Gwen	1.671–2.522	2.144	0.193	91
Bathymodiolus				
Logatchev	1.515–2.219	1.802	0.171	43
Bathymodiolus				
Snake Pit	1.624–2.087	1.930	0.127	19

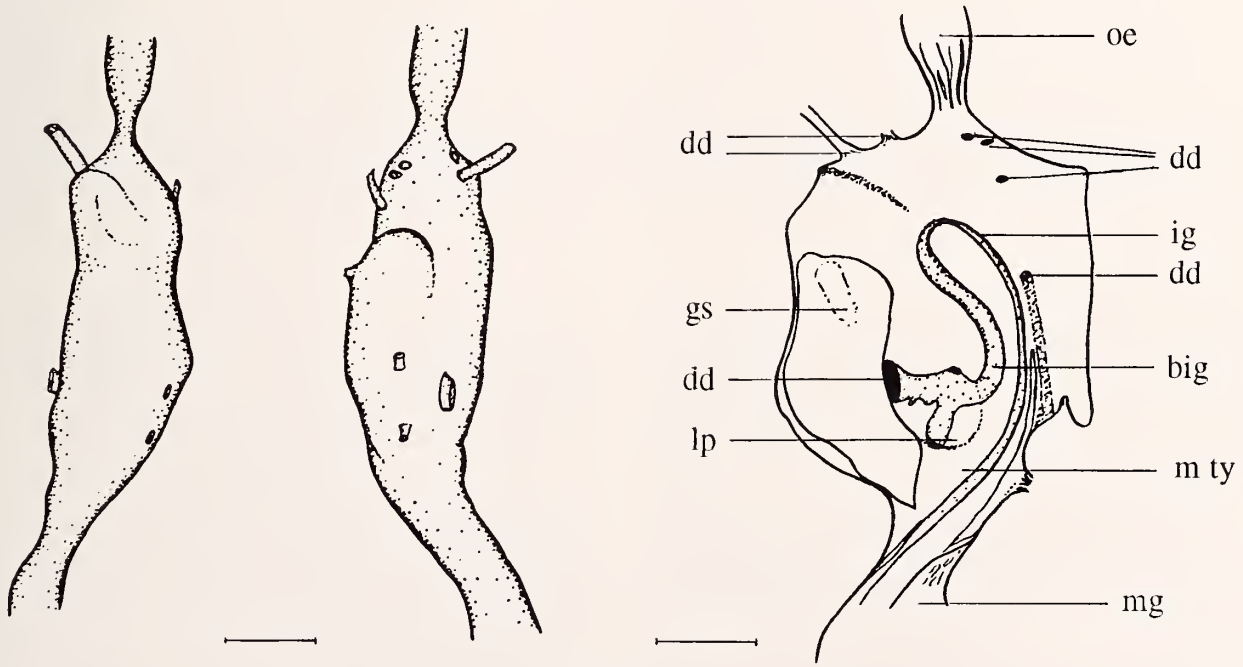

Figure 66

Bathymodiolus sp., stomach of specimen on Figure 16. Left,: dorsal-lateral view; middle, ventral view; right, stomach opened dorsally. oe, esophagus; dd, digestive diverticula duct (entrance); ig, intestinal groove; mty, major typhlosole; gs, gastric shield; big, beginning of intestinal groove; lp, left pouch; mg, midgut. Scale: 2 mm.

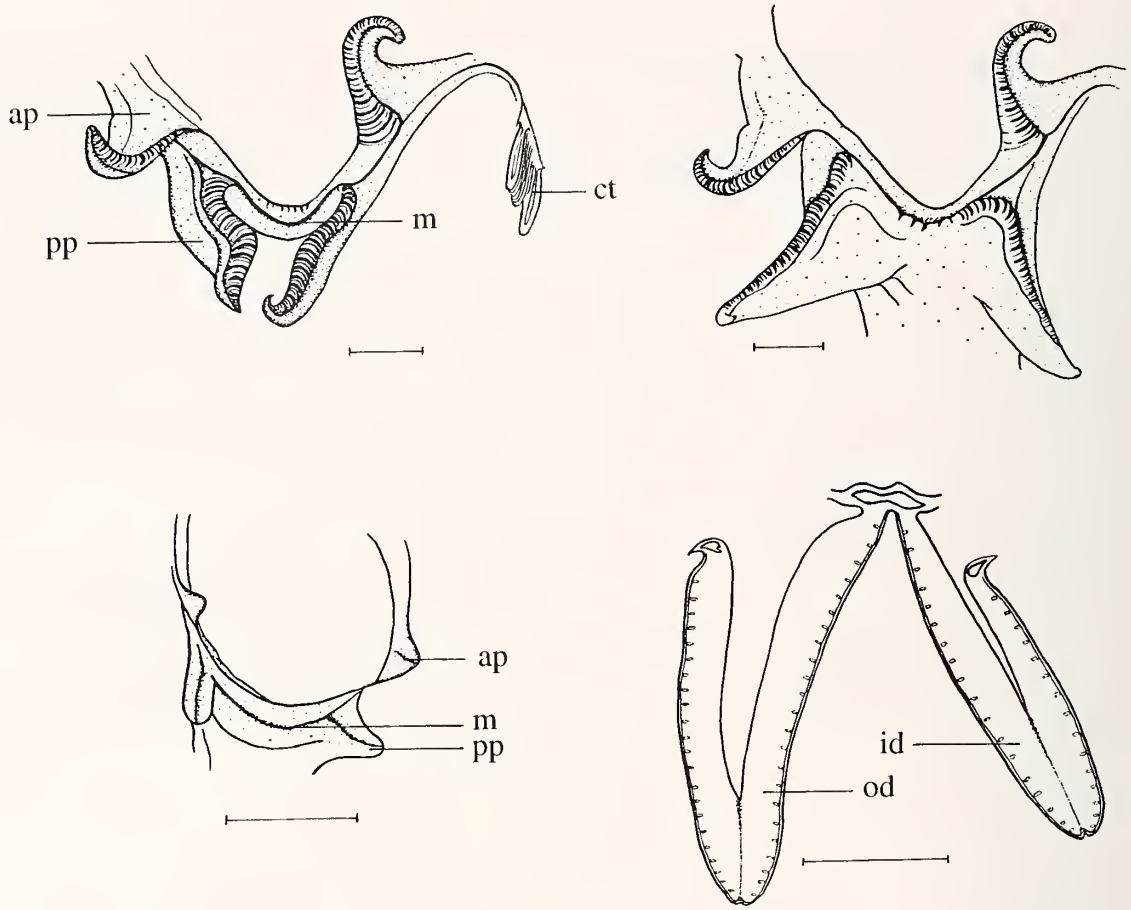

Figure 67

Bathymodiolus sp., upper row: labial palps of adult specimens, viewed from anterior end; below left: labial palps of juvenile specimens; below right: cross-section of ctenidia from the region anterior to pericardium; ap, anterior palps; pp, posterior palps; od, outer demibranch; id, inner demibranch; Scale: 2 mm; ctenidia: 1 mm.

A systematical subsampling procedure was realized by dividing the length range into 11 classes (20–30 mm; 110–120 mm; larger than 120 mm) and taking 10 individuals in each class when possible, in order to give the same weight to each size category. Table 3 gives length/height ratios calculated for each subsample (see also Figure 68).

Length/height ratios of *B. **azoricus*** and *Bathymodiolus* sp. were compared by means of a one-way ANOVA. Individuals of *B. puteoserpentis* from Snake Pit were not included in this comparison due to their low numbers. Length/height ratios are significantly different (P = 0.0001).

For *B. **azoricus,*** pairwise comparisons using the Fisher PLSD test show no significant differences (significance level 95%) between Isabel and Sintra, between Eiffel Tower and PP5, and between Statue of Liberty and Menez Gwen:

	Fisher PLSD
Isabel vs. Sintra	0.059
Eiffel Tower vs. PP5	0.060
Statue of Liberty vs. Menez Gwen	0.064

All other pairwise comparisons show significant differences at the 95% level. In particular, pairwise comparisons between each subsample of *B. **azoricus*** and the subsample of *Bathymodiolus* sp. from the Logatchev field indicate that length/height ratios in both species are significantly different at the 95% level.

Length/height ratios of *B. puteoserpentis* from Snake Pit and *Bathymodiolus* sp. from Logatchev are significantly different (Mann-Whitney U test, P = 0.003). However, if we consider only individuals larger than 50 mm in length (because the Snake Pit sample contains exclusively such large individuals), mean length/height ratios

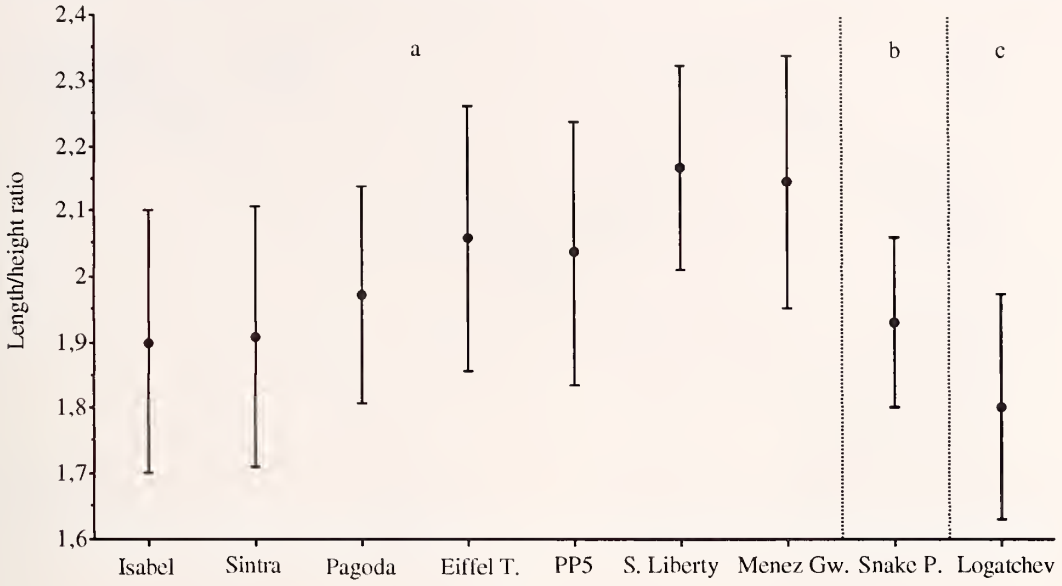

Figure 68

Length-height ratios of a. *Bathymodiolus* ***azoricus*** Cosel & Comtet, sp. nov. from different sites; b. *Bathymodiolus puteoserpentis* Cosel, Métivier & Hashimoto, 1994; c. *Bathymodiolus* sp. from Logatchev. Bars are 1 SD.

of *B. puteoserpentis* and *Bathymodiolus* sp. (respectively 1.930 ± 0.127 and 1.944 ± 0.140) do not differ significantly (Mann-Whitney U test, $P = 1$).

Anterior Part Length

Additional measurements of the anterior part length (i.e., the distance from the anterior margin to the umbo) were taken on 130 individuals of *Bathymodiolus* ***azoricus*** (75 specimens from Menez Gwen, 32 from Pagoda, and 23 from Eiffel Tower); 22 individuals of *Bathymodiolus* sp.; and seven individuals of *B. puteoserpentis*. Measurements from Pagoda and Eiffel Tower were pooled and considered as representing *B.* ***azoricus*** from Lucky Strike. Total length/anterior part length ratios were then calculated and compared between the three species (Table 4 and Figure 69).

Bathymodiolus ***azoricus*** is clearly distinct from *Bathymodiolus* sp. and *B. puteoserpentis* with a total length/anterior part length ratio being two times higher for *B.* ***azoricus***. Total length/anterior part length ratios in *B.* ***azoricus*** differ significantly between Lucky Strike and Menez Gwen (Student t test $P = 0.0004$), whereas in *Bath-*

Table 4

Total length/anterior part length ratios in *Bathymodiolus* ***azoricus***, *Bathymodiolus* sp. and *B. puteoserpentis* from different localities of the MAR. n: sample size.

	Total length/anterior part length ratio			
	Mean	Standard deviation	n	Total length range (mm)
B. ***azoricus***				
Menez Gwen	13.785	3.108	75	13.10–109.70
Lucky Strike	11.782	3.044	55	38.30–101.40
Bathymodiolus sp.				
Logatchev	6.610	0.936	22	36.90–123.40
B. puteoserpentis				
Snake Pit	7.250	0.799	7	98.20–136.10

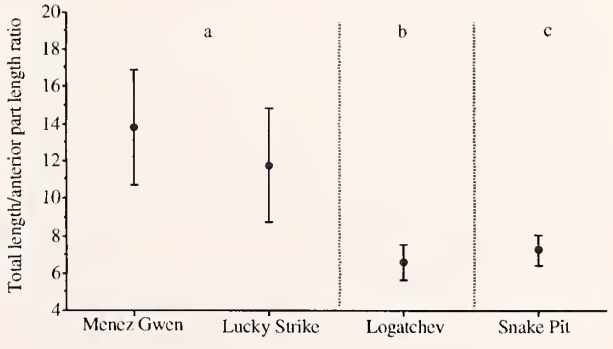

Figure 69

Ratios of total shell length/anterior part length of a. *Bathymodiolus* ***azoricus*** Cosel & Comtet, sp. nov. from Lucky Strike and Menez Gwen; b. *Bathymodiolus* sp. from Logatchev; c. *Bathymodiolus puteoserpentis* Cosel, Métivier & Hashimoto, 1994 from Snake Pit. Bars are 1 SD.

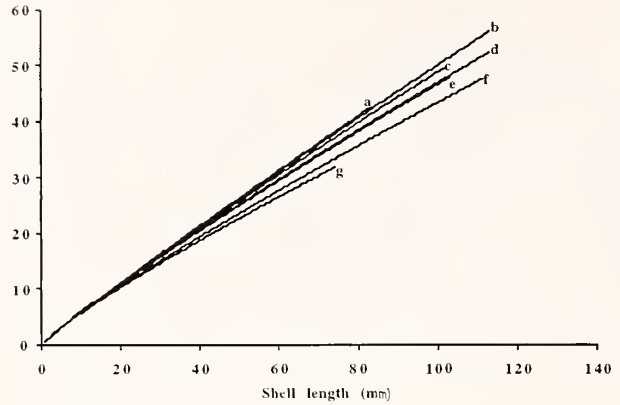

Figure 70

Shell height (H) vs. shell length (L) for *Bathymodiolus* ***azoricus*** from several sites of the Lucky Strike and Menez Gwen hydrothermal fields. Each curve represents the allometric model ($y = ax^b$) (Teissier, 1948) fitted to the observed data (not shown).

a	Sintra	$H = 0.6838L^{0.9346}$	$r^2 = 0.9967$
b	Isabel	$H = 0.6871L^{0.9317}$	$r^2 = 0.9968$
c	Pagoda	$H = 0.7213L^{0.9158}$	$r^2 = 0.9954$
d	Eiffel Tower	$H = 0.7671L^{0.8939}$	$r^2 = 0.9969$
e	PP5	$H = 0.7504L^{0.8973}$	$r^2 = 0.9969$
f	Menez Gwen	$H = 0.7724L^{0.8752}$	$r^2 = 0.9958$
g	Statue of Liberty	$H = 0.7906L^{0.8592}$	$r^2 = 0.9967$

ymodiolus sp. and *B. puteoserpentis* they are significantly different at the 95% level but not at the 99% level (Mann-Whitney U test, $P = 0.0415$).

Remarks: The biometry study shows a great intersite (and interfield) variability of the shell shape in *Bathymodiolus* ***azoricus***. However, from length/height ratio comparisons, three groups can be distinguished, corresponding to three different morphs: Isabel/Sintra, Eiffel Tower/PP5, and Statue of Liberty/Menez Gwen, the mussels from the latter being the most elongate (i.e., having the highest length/height ratio) (Figure 68). Specimens from Pagoda have a length/height ratio intermediate between the two first groups but can be associated with the first one (Isabel/Sintra). This variability is difficult to explain but could be due to intersite differences in the physico-chemical environment (temperature, fluid composition, etc.). Biotic factors such as mussel density could also affect the shell shape.

Despite such variability, *B.* ***azoricus*** of each site could be distinguished from *Bathymodiolus* sp. by the much higher length/height ratio, i.e., having a more elongate shell. The length/height ratio for *B. puteoserpentis,* intermediate between those of *B.* ***azoricus*** and *Bathymodiolus* sp., is not significantly different from that of *Bathymodiolus* sp., when considering a similar length range (>50 mm).

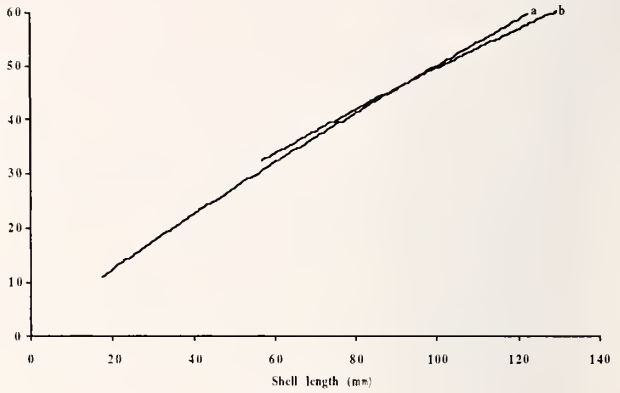

Figure 71

Shell height (H) vs. shell length (L) for *Bathymodiolus* sp. (a) from the Logatchev hydrothermal field and *Bathymodiolus puteoserpentis* (b) from the Snake Pit hydrothermal field. Each curve represents the allometric model ($y = ax^b$) (Teissier, 1948) fitted to the observed data (not shown).

a	$H = 0.9143L^{0.8679}$	$r^2 = 0.9928$	
b	$H = 1.5232L^{0.7552}$	$r^2 = 0.9033$	

Comparisons of the total length/anterior part length ratios confirm the morphological similarity between *B. puteoserpentis* and *Bathymodiolus* sp., whereas *B.* ***azoricus*** is well distinguished from these two species by the much shorter anterior part, i.e., by an almost terminal umbo (Figure 69).

DISCUSSION

From the study of the gross anatomy, it is evident that unlike the type species of the genus, *Bathymodiolus thermophilus,* all other large hydrothermal vent or cold seep mussels subsequently described under the generic name *Bathymodiolus* or still under study (Craddock et al., 1995; Cosel & Olu, 1998; Gustafson et al., 1998) have one major character complex which is distinct from *B. thermophilus:* the absence of an inner mantle fold fusion and the reduction of the valvular siphonal membrane to a short transverse sheet at the posterior end of the animal. In these mussels, the "ventral gape" stretches over the whole length of the shell, whereas in *B. thermophilus,* the fusion encloses the mantle cavity to a large extent, leaving only a rather small byssal and inhalent mantle opening. In connection with this, the other *Bathymodiolus* species lack a lateral muscular ridge on mantle lobes and visceral mass, and a posterior branchial septum, which in *B. thermophilus* divides more completely the excurrent and incurrent chambers. However, other "unusual" characters found by Kenk & Wilson (1985) in *B. thermophilus* (e.g., thick and very large ctenidia, very large auricles,

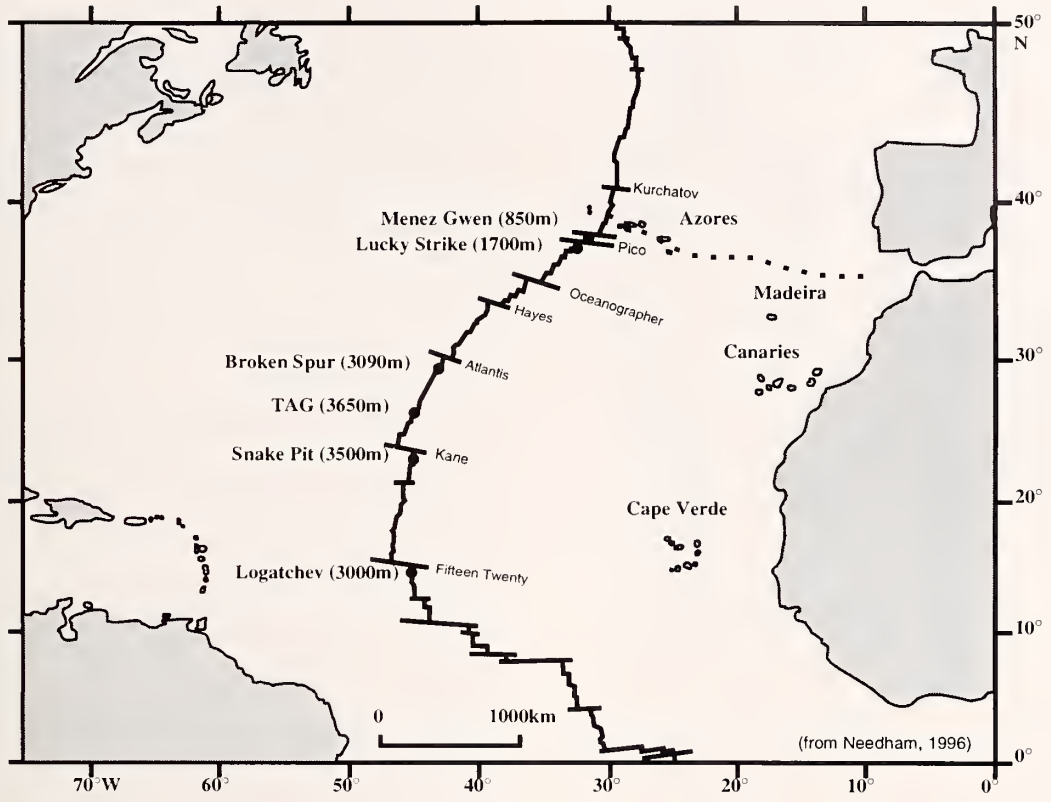

Figure 72

Map of the northern part of the Atlantic showing the known hydrothermal fields and transform faults on the MAR (taken from Needham, 1996).

symbiose with chemo-autotrophic bacteria) are present in the other species. The difference in the degree of mantle fusion, already discussed by Cosel et al. (1994), could lead to the introduction of a new genus to separate these species from *B. thermophilus*.

However, if one looks at Mytilidae of other genera of which the anatomy is described, none is known to have a similar ventral mantle fusion like *Bathymodiolus thermophilus*. This feature, only known from a hydrothermal vent mussel, has certainly developed after the separation of the *B. thermophilus* stock on the East Pacific Rise, and is a derived character, and only by chance, the most apomorphic species of the large mussels from hydrothermal vents was discovered and described first and is hence the name-bearer of the genus. Species without inner mantle fold fusion and very short valvular siphonal membrane are much more plesiomorphic in contrast to the apomorphic character of the fused inner mantle folds in the type species of the genus *Bathymodiolus*. A new supraspecific taxon cannot be introduced based on this.

Moreover, an electrophoretic analysis with 18 enzymes by Craddock et al. (1995) revealed a genetic distance D (Nei, 1978) of 1.865 between *Bathymodiolus thermophilus* and the Snake Pit mussel (now *B. puteoserpentis*) and 1.871 between *B. thermophilus* and the Lucky Strike mussel (now *B. **azoricus***); the distance between *B. puteoserpentis* and *B. **azoricus*** is 1.179. The genetic distances (D values) between these three hydrothermal vent mussels are within the values usually found with species-level separation (Craddock et al., 1995).

Neither the morphological differences nor the genetic distance are a reason for introducing a new genus for the two species here treated, and as a consequence we maintain them in the genus *Bathymodiolus*.

Another difference, the more complicated stomach and the intestinal coiling in the species here treated versus the simple stomach without left pouch and with only three pairs of entering digestive gland ducts, and the straight digestive tract in *B. thermophilus* underlines that the latter is more apomorphic: it shows that the degree of direct filter feeding with digestion via the digestive tract has diminished in favor of nutrition by bacteria, whereas in our species, direct feeding remains more important.

Some Zoogeographic Remarks

Two species (and one population not recognized as full species) of *Bathymodiolus* associated with hydro-

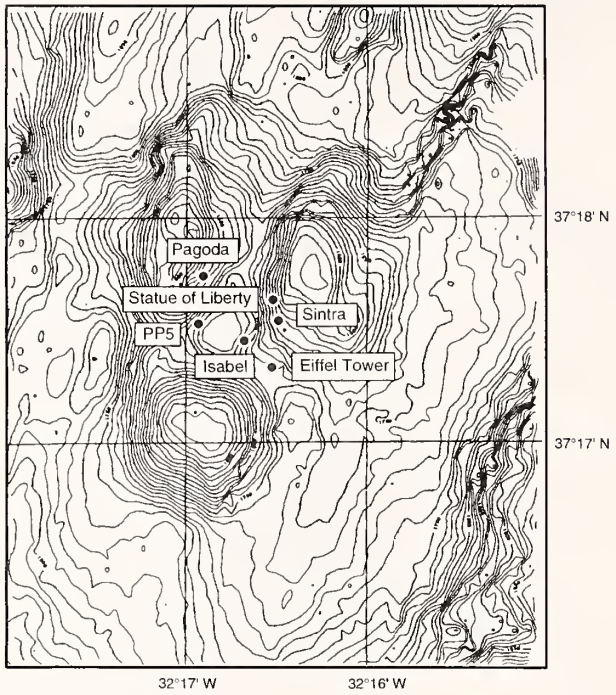

Figure 73

Map of the Lucky Strike hydrothermal field.

thermal activity are known to date from the MAR, but only a single species is found at one particular site. Their respective geographic range is limited to a few hydrothermal fields. The northernmost species is ***B. azoricus,*** which occurs at the Lucky Strike and Menez Gwen vent fields (37°17′N and 37°50′N, respectively). *B. puteoserpentis* inhabits the Snake Pit field (23°N), and *Bathymodiolus* sp. occurs on the Logatchev hydrothermal field (14°45′N). It was found that the morphological differences between the populations of Lucky Strike and Menez Gwen, on the one hand, and that of Snake Pit, on the other hand, are the most numerous and most obvious and have led us to distinguish two species. Differences between the Snake Pit population and the Logatchev population are less apparent but observable. Mussels from the Broken Spur hydrothermal field (29°10′N) are morphologically close to *B. puteoserpentis,* and were provisionally identified with this species by the first author. However, it is necessary to be cautious since the morphological analysis was conducted on only two broken shells. One specimen of a mytilid was collected on the TAG hydrothermal field (26°N, 3640–3680 m), but remains to be identified (P. Rona, personal communication). The endemism at specific level for the Mytilidae of the MAR was explained by a combination of depth effect and the role of transform faults on larval dispersal (Craddock et al., 1995; Van Dover, 1995; Van Dover et al., 1996).

The bathymetric ranges observed for each species indicate that the MAR mussels occupy two discrete bathymetric intervals. ***B. azoricus*** is restricted to shallower hydrothermal fields (850 m and 1700 m), whereas *B. puteoserpentis* and *Bathymodiolus* sp., as well as the mussels from Broken Spur and TAG, occur at depths exceeding 3000 m. The examination of ultrajuvenile specimens and larvae in the Protoconch II stage from the Logatchev hydrothermal field showed that at least two different bivalve species are present, most probably the other also a mussel, so it is probable that another mytilid species reaches the site as planktonic larvae but does not find adequate conditions for settling.

Transform faults, which are numerous and various along the MAR (Needham, 1996), have been considered as barriers to the dispersal of vent invertebrates (e.g., Craddock et al., 1995; Van Dover, 1995; Van Dover et al., 1996) but their role may depend on the dispersal strategies of each species. Hydrothermal vent mytilids, and especially the species from the MAR, have a planktotrophic larval development, as inferred from size and morphology of the protoconch II (Lutz et al., 1980; Cosel et al., 1994; this paper), which allows the larvae to remain in the plankton for at least several weeks and to be widely dispersed by currents, after being driven by the plume to the level of lateral spreading several hundred meters above the bottom (Kim et al., 1994; Mullineaux & France, 1995; Mullineaux et al., 1995). One might expect that such a dispersal strategy would permit mytilid larvae to colonize vent fields separated by great distances regardless of transform faults or other physiographic features. Thus, the 45 km offset of the Pico transform fault (Figure 72), which separates Lucky Strike from Menez Gwen (with a distance of 60 km), does not constitute a major obstacle for the dispersal of ***B. azoricus.*** However, if the mussels from Broken Spur are clearly identified as *B. puteoserpentis* in the future, they would be the northernmost population of the species. The presence of three major faults (Oceanographer, Hayes, and Atlantis faults) between Lucky Strike and Broken Spur is a possible factor for differentiation between both areas. The Kane fracture zone, with an offset of 145 km, which separates Snake Pit and TAG/Broken Spur, does not seem to prevent dispersal of *B. puteoserpentis,* but the Fifteen-Twenty transform fault could explain reduced exchanges between Snake Pit and Logatchev. In addition to the possible role of transform faults, the low spatial frequency of occurrence of hydrothermal fields on the MAR, estimated at one field every 175 km by German et al. (1995), could limit the dispersal by lack of step-by-step processes. However, the occurrence of several other vent species (e.g., the alvinocaridid shrimp, *Chorocaris chacei* (Williams & Rona, 1986), the bythograeid crab, *Segonzacia mesatlantica* (Williams, 1988), the gastropod, *Protolira valvatoides* Warén & Bouchet, 1993, and the commensal polynoid

polychaete, *Branchipolynoe seepensis*), with a wider geographical range on the MAR (Van Dover et al., 1996; Gebruk et al., 1997; Segonzac, personal communication), suggests that dispersal could occur along the entire MAR despite transform faults, and that these are not the only factors controlling the mytilid geographical distribution. Further investigations at intermediate depths and latitudes will allow us to precisely determine the role of depth and topography of the ridge in the distribution of mytilid species along the MAR.

ACKNOWLEDGMENTS

We would like to express our sincere gratitude to C. Langmuir (Lamont-Doherty Earth Observatory), Y. Fouquet, D. Desbruyères and A.-M. Alayse (IFREMER Brest), D. Prieur (Station Biologique de Roscoff), and all the participants of the LUCKY STRIKE 1993, LOGACHEV-7, *Akademik Mstislav Keldysch* cruise 35, DIVA 1, DIVA 2, and MICROSMOKE expeditions. We thank M. Segonzac (CENTOB, French National Sorting Center, IFREMER, Brest) and L. I. Moskalev (P. P. Shirshov Institute of Oceanology) for placing the collected material at our disposal. We are grateful to S. Gofas and two anonymous referees for critically reading the manuscript and giving hints to improve it. For help in preparing the specimens for SEM photos, we kindly thank S. Gofas; the assistance of Mrs. Grassé (CIME, Dept. MEB, Université Paris-VI) for the SEM photos is gratefully acknowledged. This work was supported in part by a contribution from the Programme "DORSALES" (Contrat IFREMER 961410106), in part by the European Community (MAST3-CT95-0040 AMORES), and in part by INTAS (International Association for the Promotion of Cooperation with Scientists from the Independent States of the former Soviet Union) (project number 94-0592).

LITERATURE CITED

Batuyev, B. N., A. G. Krotov, V. F. Markov, G. A. Cherkashev, S. G. Krasnov & Y. D. Lisitsyn. 1994. Massive sulphide deposits discovered and sampled at 14°45′N, Mid-Atlantic ridge. BRIDGE Newsletter 6:6–10.

Childress, J. J. & C. R. Fisher. 1992. The biology of hydrothermal vent animals: physiology, biochemistry, and autotrophic symbioses. Oceanography and Marine Biology Annual Review 30:337–441.

Comtet, T. 1994. Etude de la croissance allométrique et de la structure des populations de modioles sur la zone hydrothermale Lucky Strike (37°17′N sur la ride médio-atlantique). Master's Thesis (DEA, Diplome d'Etudes Approfondis), Université de Bretagne Occidentale, Brest.

Cosel, R. von & K. Olu. 1998. Gigantism in Mytilidae. A new *Bathymodiolus* from cold seep areas on the Barbados accretionary Prism. Comptes rendus de l'Academie des Sciences, Paris, Sciences de la vie, 1998, 321:655–663.

Cosel, R. von, B. Métivier & J. Hashimoto. 1994. Three new species of *Bathymodiolus* (Bivalvia: Mytilidae) from hydrothermal vents in the Lau Basin and the North Fiji Basin, Western Pacific, and the Snake Pit area, Mid-Atlantic Ridge. The Veliger 37(4):374–392.

Craddock, C., W. R. Hoeh, R. G. Gustafson, R. A. Lutz, J. Hashimoto & R. J. Vrijenhoek. 1995. Evolutionary relationships among deep-sea mytilids (Bivalvia: Mytilidae) from hydrothermal vents and cold-water methane/sulfide seeps. Marine Biology 121:477–485.

Desbruyères, D., A.-M. Alayse, E. Antoine, G. Barbier, F. Barriga, M. Biscoito, P. Briand, J.-P. Brulport, T. Comtet, L. Cornec, P. Crassous, P. Dando, M.-C. Fabri, H. Felbeck, F. Lallier, A. Fiala-Médioni, J. Gonçalves, F. Ménard, J. Kerdoncuff, J. Patching, L. Saldanha & P.-M. Sarradin. 1994. New information on the ecology of deep-sea vent communities in the Azores Triple Junction area: preliminary results of the Diva 2 cruise (May 31–July 4, 1994). Inter Ridge News 3:18–19.

Fiala-Médioni, A., C. Cavanaugh, P. Dando & C. L. Van Dover. 1996. Symbiotic mussels from the Mid-Atlantic Ridge: adaptations to trophic resources. Journal of Conference Abstracts 1:788.

Fouquet, Y., H. Ondréas, J-L. Charlou, J.-P. Donval, J. Radford-Knoëry, I. Costa, N. Lourenço & M. K. Tivey. 1995. Atlantic lava lakes and hot vents. Nature 377:201.

Gebruk, A. V., S. V. Galkin, A. L. Vereshchaka, L. I. Moskaley & A. J. Southward. 1997. Ecology and biogeography of the hydrothermal vent fauna of the Mid-Atlantic Ridge. Advances in Marine Biology 32:93–144.

German, C. R., E. T. Baker & G. Klinkhammer. 1995. Regional setting of hydrothermal activity. Pp. 3–15 in L. M. Parson, C. L. Walker & D. R. Dixon (eds.), Hydrothermal Vents and Processes. Geological Society: Boulder, Colorado.

Gustafson, R. G., R. D. Turner, R. A. Lutz & R. C. Vrijenhoek. 1998. A new genus and five new species of mussels (Bivalvia: Mytilidae) from deep-sea sulfide/hydrocarbon seeps in the Gulf of Mexico. Malacologia 40(1–2):63–112.

Hashimoto, J. & T. Okutani. 1994. Four new mytilid mussels associated with deepsea chemosynthetic communities around Japan. Venus (Japanese Journal of Malacology) 53(2):61–83.

Kenk, V. C. & B. R. Wilson. 1985. A new mussel (Bivalvia: Mytilidae) from hydrothermal vents in the Galapagos Rift zone. Malacologia 26(1-2):253–271.

Kim, S. L., L. S. Mullineaux & K. R. Helfrich. 1994. Larval dispersal via entrainment into hydrothermal vent plumes. Journal of Geophysical Research C 99:12655–12665.

Le Pennec, M. & A. Hily. 1984. Anatomie, structure et ultrastructure de la branchie d'un Mytilidae des sites hydrothermaux du Pacifique oriental. Oceanologica Acta 7(4):517–523.

Lutz, R. A., D. Jablonski, D. C. Rhoads & R. D. Turner. 1980. Larval dispersal of a deep-sea hydrothermal vent bivalve from the Galapagos Rift. Marine Biology 57:127–133.

Mullineaux, L. S. & S. C. France. 1995. Dispersal mechanisms of deep-sea hydrothermal vent fauna. Pp. 408–424 in S. E. Humphris, R. A. Zierenberg, L. S. Mullineaux, & R. E. Thomson (eds.), Seafloor Hydrothermal Systems: Physical, Chemical, Biological, and Geological interactions. American Geophysical Union: Washington, DC.

Mullineaux, L. S., P. H. Wiebe & E. Baker. 1995. Larvae of benthic invertebrates in hydrothermal vent plumes over Juan de Fuca Ridge. Marine Biology 122:585–596.

Murton, B. J., C. Van Dover & E. Southward. 1995. Geological setting and ecology of the Broken Spur hydrothermal

vent field: 29°10′N on the Mid-Atlantic Ridge. Pp. 33–41 in L. M. Parson, C. L. Walker & D. R. Dixon (eds.), Hydrothermal Vents and Processes. Geological Society: Boulder, Colorado.

NEEDHAM, H. D. 1996. Some features of the North America-Africa plate boundary. Journal of Conference Abstracts 1: 834–835.

NEI, M. 1978. Estimation of average heterozygosity and genetic distance from a small number of individuals. Genetics 89: 583–590.

TEISSIER, G. 1948. La relation d'allométrie. Sa signification statistique et biologique. Biometrics 4:14–53.

VAN DOVER, C. L. 1995. Ecology of Mid-Atlantic Ridge hydrothermal vents. Pp. 257–294 in L. M. Parson, C. L. Walker & D. R. Dixon (eds.), Hydrothermal Vents and Processes. Geological Society: Boulder, Colorado.

VAN DOVER, C. L., D. DESBRUYÈRES, M. SEGONZAC, T. COMTET, L. SALDANHA, A. FIALA-MÉDIONI & C. LANGMUIR. 1996. Biology of the Lucky Strike hydrothermal field. Deep-Sea Research I 43:1509–1529.

Note Added in Proof: After acceptance of this manuscript, two other papers with descriptions of mussels from hydrothermal vents and cold seeps were published: Cosel & Olu (1998) and Gustafson et al. (1998), which unfortunately could not be considered here. In total, six new species were described, among them four in the genus *Bathymodiolus*. This augments the total number of described and named species of hydrothermal vent and cold seep mussels to 13.